

Old Dominion University

## ODU Digital Commons

---

Electrical & Computer Engineering Theses &  
Dissertations

Electrical & Computer Engineering

---

Summer 2005

# Electromagnetic Wave Propagation Prediction for Wireless Networks Inside Boeing Fuselages

Mennatoallah Youssef  
*Old Dominion University*

Follow this and additional works at: [https://digitalcommons.odu.edu/ece\\_etds](https://digitalcommons.odu.edu/ece_etds)



Part of the [Aeronautical Vehicles Commons](#), [Computational Engineering Commons](#), [Digital Communications and Networking Commons](#), [Electromagnetics and Photonics Commons](#), and the [Signal Processing Commons](#)

---

### Recommended Citation

Youssef, Mennatoallah. "Electromagnetic Wave Propagation Prediction for Wireless Networks Inside Boeing Fuselages" (2005). Master of Science (MS), Thesis, Electrical & Computer Engineering, Old Dominion University, DOI: 10.25777/5hdw-rr14  
[https://digitalcommons.odu.edu/ece\\_etds/586](https://digitalcommons.odu.edu/ece_etds/586)

This Thesis is brought to you for free and open access by the Electrical & Computer Engineering at ODU Digital Commons. It has been accepted for inclusion in Electrical & Computer Engineering Theses & Dissertations by an authorized administrator of ODU Digital Commons. For more information, please contact [digitalcommons@odu.edu](mailto:digitalcommons@odu.edu).

**ELECTROMAGNETIC WAVE PROPAGATION PREDICTION FOR  
WIRELESS NETWORKS INSIDE BOEING FUSELAGES**

by

Mennatoallah Youssef  
B.S. Electrical Engineering, Spring 2004, Old Dominion University

A Thesis Submitted to the Faculty of  
Old Dominion University in Partial Fulfillment of the  
Requirement for the Degree of

MASTER OF SCIENCE

ELECTRICAL ENGINEERING

OLD DOMINION UNIVERSITY

August 2005

Approved by:

\_\_\_\_\_  
Linda L. Vahala (Director)

\_\_\_\_\_  
Hani Elsayed-Ali (Member)

\_\_\_\_\_  
Ravindra Joshi (Member)

## **ABSTRACT**

### **ELECTROMAGNETIC WAVE PROPAGATION PREDICTION FOR WIRELESS NETWORKS INSIDE BOEING FUSELAGES**

Mennatoallah M. Youssef  
Old Dominion University, 2005  
Director: Dr. Linda Vahala

Commercial grade software is intended for electromagnetic predictions within office buildings; it was used to develop models to analyze propagation inside airplane fuselages. This study shows that Wireless XGTD and Insite software can accurately predict power propagation within airplane fuselages. Current work uses fuselage models, which contain additional internal components. A comparison was made between empty and full fuselage to examine the effects of internal components. Two propagation model types [Fast 3D and Full 3D] were also compared for accuracy to experimental study. It was concluded that completed fuselages are suggested for further simulation study as well as that the Full 3D propagation method is more accurate than Fast 3D. The software could qualitatively predict electromagnetic propagation inside the aircraft cabin environment.

## **DEDICATION**

To Mother and Father, Hanaa and Mohamed Youssef and  
Siblings, Louay, Eyad, and Hebbatoallah  
for their unconditional love and support.

In memory of my uncle, Hani A. Khalil

## **ACKNOWLEDGEMENTS**

I would like to thank my advisor Dr. Linda Vahala for her assistance in completing this thesis. Her encouragement and academic support helped further this thesis. I would also like to acknowledge Dr. John Beggs as my mentor at NASA Langley, and the other researchers at the Langley HIRF lab as well the RF'n fun research group at Old Dominion University. I would also like to acknowledge Dr. Donald Swift and Professor Sondra Swift for their aid in completing this thesis

I would like to acknowledge my parents, Hanaa and Mohamed Youssef.

## TABLE OF CONTENTS

<b>LIST OF FIGURES .....</b>	<b>VII</b>
<b>LIST OF EQUATIONS .....</b>	<b>IX</b>
<b>LIST OF TABLES .....</b>	<b>X</b>
<b>I. INTRODUCTION .....</b>	<b>1</b>
GROWTH AND ATTRACTIVENESS OF WIRELESS NETWORKS .....	1
USER SPECIFIC ADVANTAGES .....	1
PILOT SPECIFIC ADVANTAGES .....	2
CURRENT IMPLEMENTATIONS .....	2
MODELING AND SIMULATION .....	3
OBJECTIVES .....	4
<b>II. BACKGROUND .....</b>	<b>5</b>
WLAN.....	5
<i>Signal Modulation</i> .....	5
<i>Operation Frequency and Data Rate Transfer</i> .....	7
SIGNAL PROPAGATION EFFECTS .....	7
PREVIOUS EXPERIMENTAL STUDY .....	9
<i>Limitation in Experimental Study</i> .....	10
<i>Experimental Setup</i> .....	11
<i>Experimental Results</i> .....	13
ELECTROMAGNETIC MODELING.....	15
<b>III. SIMULATION.....</b>	<b>18</b>
PROPAGATION METHODS .....	18
<i>Urban Canyon Model</i> .....	19
<i>Fast 3D Urban Model</i> .....	20
<i>Full 3D Model</i> .....	22
FUSELAGE MODELS .....	23
<i>Rectangular Models</i> .....	23
<i>Cylindrical Models</i> .....	28
<i>Importation</i> .....	30
ANTENNAS, RECEIVERS, & TRANSMITTERS .....	31
ELECTRIC FIELD CALCULATIONS .....	35
<i>Urban Canyon Method:</i> .....	35
<i>Fast 3D and Full 3D Method:</i> .....	38
POWER CALCULATION .....	41
<b>IV. ANALYSIS OF DATA .....</b>	<b>43</b>
INTERNAL COMPONENT ANALYSIS: EMPTY FUSELAGE VERSUS COMPLETED FUSELAGE.....	45
<i>Analysis:</i> .....	48
<i>Analysis:</i> .....	52
PROPAGATION MODEL ANALYSIS: FAST 3D METHOD VERSUS FULL 3D METHOD .....	53

<i>Analysis:</i> .....	56
<i>Analysis:</i> .....	63
POSSIBLE REASONS FOR DIFFERENCES IN EXPERIMENTAL DATA VERSUS SIMULATION ...	63
SUMMARY TABLES .....	65
<b>V. CONCLUSIONS .....</b>	<b>66</b>
<b>REFERENCES.....</b>	<b>67</b>
<b>VITA.....</b>	<b>68</b>

## LIST OF FIGURES

FIGURE 1: OFDM EFFICIENT USE OF BANDWIDTH.....	6
FIGURE 2: EXAMPLE OF DIFFRACTION AND REFLECTION OF SIGNALS OFF AN ARBITRARY BUILDING. [2].....	8
FIGURE 3: ORINOCO AP2000.....	9
FIGURE 4: EXPERIMENTAL SETUP.....	11
FIGURE 5: SEAT LAYOUT OF BOEING 747 WITH AP LOCATION.....	12
FIGURE 6: SEAT LAYOUT OF BOEING 777 WITH AP LOCATION.....	12
FIGURE 7: SEAT LAYOUT OF BOEING 767 WITH AP LOCATION.....	12
FIGURE 8: RF POWER READING FOR SPECTRUM ANALYZER AND CLIENT CARD.....	14
FIGURE 9: EXPERIMENTAL RESULT OF RF POWER PROPAGATION OF B747.....	14
FIGURE 10: EXPERIMENTAL RESULT OF RF POWER PROPAGATION OF B777.....	15
FIGURE 11: EXPERIMENTAL RESULT OF RF POWER PROPAGATION OF B767.....	15
FIGURE 12: YEE'S LATTICE[7]. .....	16
FIGURE 13: RECTANGULAR MODELS (A) GENERIC BOEING MODEL (B) BOEING 747.....	24
FIGURE 14: CYLINDRICAL MODELS. ....	24
FIGURE 15: RECTANGULAR MODEL B767A. ....	26
FIGURE 16: RECTANGULAR MODEL B767B. ....	26
FIGURE 17: RECTANGULAR MODEL B777A. ....	27
FIGURE 18: RECTANGULAR MODEL B777AB.....	27
FIGURE 19: BOEING CAD DRAWING USED FOR DIMENSIONING. ....	28
FIGURE 20: SEAT ARRANGEMENTS.....	29
FIGURE 21: BOEING 767 MODEL DEPICTED IN SOLIDWORKS ®. ....	30
FIGURE 22: FUSELAGE MODELS IN WIRELESS INSITE. ....	31
FIGURE 23: EXAMPLE OF WI SCREENSHOT OF ANTENNA PROPERTIES.....	32
FIGURE 24: WI SCREENSHOT OF BASIC TRANSMITTER PROPERTIES.....	32
FIGURE 25: 3D ANTENNA PATTERN (A) OMNIDIRECTIONAL ANTENNA.....	33
FIGURE 26: WI DEPICTION OF FUSELAGE WITH TRANSMITTER AND RECEIVERS. ....	34
FIGURE 27: RECEIVER LAYOUT COMPARED TO EXPERIMENTAL STUDY.....	34
FIGURE 28: WIRELESS INSITE SPHERICAL COORDINATE SYSTEM. ....	35
FIGURE 29: B747 (A) 802.11A STANDARD (B) 802.11B STANDARD. ....	45

FIGURE 30: B767 (A) 802.11A STANDARD (B) 802.11B STANDARD. ....	46
FIGURE 31: B777 (A) 802.11A STANDARD (B) 802.11B STANDARD. ....	47
FIGURE 32: B747 (A) 802.11A STANDARD (B) 802.11B STANDARD. ....	49
FIGURE 33: B767 (A) 802.11A STANDARD (B) 802.11B STANDARD. ....	50
FIGURE 34: B777 (A) 802.11A STANDARD (B) 802.11B STANDARD. ....	51
FIGURE 35: FAST 3D AND FULL 3D COMPARISON B747. ....	53
FIGURE 36: FAST 3D AND FULL 3D COMPARISON B767. ....	54
FIGURE 37: FAST 3D AND FULL 3D COMPARISON B777. ....	55
FIGURE 38: COMPARING 11A AND 11B STANDARD FOR B747.....	58
FIGURE 39: COMPARING 11A AND 11B STANDARD FOR B767.....	60
FIGURE 40: COMPARING 11A AND 11B STANDARD FOR B777.....	62
FIGURE 41: PROPAGATION PATH IN B777 [FRONT VIEW].....	64
FIGURE 42: PROPAGATION PATH IN B777 [SIDE VIEW].....	64

## LIST OF EQUATIONS

EQUATION 1: MAXWELL'S TIME DEPENDENT CURL EQUATIONS [7].....	16
EQUATION 2: ELECTRIC FIELD IN FREE SPACE.....	35
EQUATION 3: ELECTRIC FIELD IN THETA DIRECTION .....	36
EQUATION 4: ELECTRIC FIELD IN PHI DIRECTION .....	36
EQUATION 5: TOTAL ELECTRIC FIELD .....	37
EQUATION 6: COMPLEX ELECTRIC FIELD FROM GROUND REFLECTION .....	37
EQUATION 7 .....	37
EQUATION 8 .....	38
EQUATION 9 .....	38
EQUATION 10 .....	38
EQUATION 11 .....	39
EQUATION 12 .....	40
EQUATION 13: ELECTRIC FIELD FOR SINGLE REFLECTION.....	40
EQUATION 14: RECEIVED POWER .....	41
EQUATION 15: TIME AVERAGED POWER .....	41
EQUATION 16: OVERLAP OF FREQUENCY SPECTRUM OF THE TRANSMITTED WAVEFORM .	42
EQUATION 17: MEAN ABSOLUTE ERROR.....	44
EQUATION 18: ROOT MEAN SQUARE ERROR.....	44

## LIST OF TABLES

TABLE 1:SUMMARY OF ACCESS POINT PARAMETERS .....	9
TABLE 2:SYSTEM REQUIREMENTS FOR WIRELESS INSITE [2].....	18
TABLE 3: URBAN CANYON MODEL CAPABILITIES [2] .....	20
TABLE 4: FAST 3D MODEL CAPABILITIES [2].....	21
TABLE 5: FULL 3D MODEL CAPABILITIES [2].....	23
TABLE 6: MAE AND RMSE DATA FOR FAST 3D .....	28
TABLE 7: MAE AND RMSE DATA FOR FULL 3D .....	28
TABLE 8: MAE AND RMSE COMPARISON FOR B747 USING FAST 3D METHOD .....	45
TABLE 9: MAE AND RMSE COMPARISON FOR B747 USING FAST 3D METHOD .....	46
TABLE 10:MAE AND RMSE COMPARISON FOR B777 USING FAST 3D METHOD .....	47
TABLE 11:MAE AND RMSE COMPARISON FOR B747 USING FULL 3D METHOD .....	49
TABLE 12: MAE AND RMSE COMPARISON FOR B767 USING FULL 3D METHOD.....	50
TABLE 13:MAE AND RMSE COMPARISON FOR B777A USING FULL 3D METHOD.....	51
TABLE 14: TABLE OF MAE AND RMSE OF B747 [FAST 3D AND FULL3D] .....	53
TABLE 15: TABLE OF MAE AND RMSE OF B767A [FAST 3D AND FULL 3D].....	54
TABLE 16: TABLE OF MAE AND RMSE OF B777 [FAST 3D AND FULL 3D] .....	55
TABLE 17: COMPARING 11A AND 11B MAE AND RMSE FOR B747 .....	58
TABLE 18: COMPARING 11A AND 11B MAE AND RMSE FOR B767 .....	60
TABLE 19: COMPARING 11A AND 11B MAE AND RMSE FOR B777 .....	62
TABLE 20: SUMMARY OF B747.....	65
TABLE 21: SUMMARY OF B767 .....	65
TABLE 22: SUMMARY OF B777 .....	65

# I. INTRODUCTION

## **Growth and Attractiveness of Wireless Networks**

In today's industrialized world, wireless networking is becoming more widespread. Companies, universities, and neighborhoods are equipping themselves with this revolutionary advancement. The average person can be connected to any network from almost any remote location.

What makes wireless networks so attractive is their easy accessibility. Particularly in today's society, an individual is dependent on the Internet for a multitude of tasks ranging from paying bills to entertainment. As this technology advances, there will be more uses for wireless networks, and they will be heavily adopted more so into everyday life [9,10].

## **User Specific Advantages**

Wireless networks are also spreading into newer unconventional environments. More specifically it is of significant interest to the aviation industry for enhanced passenger connectivity. Currently airports are equipped with wireless Internet for passengers to use. Airlines also have a desire to provide more services to their passengers as well as examine the idea of replacing wired networks. Presently these wired networks are used in aircrafts; they are unattractive due to significant additional space, weight and maintenance costs. In addition the cost of retrofitting is also very high. Wireless networks are an ideal solution to these wired networks for multiple reasons. They offer lower cost, space, and weight requirements, additionally they are much

simpler to install and retrofit. Wireless networks can be replaced and configured to fit the specific need of the airline [10].

Passengers can utilize wireless networks for personal use. Travelers can book car rentals and hotels from the airplane or send messages via the Internet. They can also change plane reservations, check weather conditions, or stay in constant contact for business meeting. The last option is especially important for companies who often send their employees on continuous travel assignments. Constant communication between the employer and employee may be necessary to successfully facilitate business transactions [9, 10].

### **Pilot Specific Advantages**

The influence of wireless networks on aircraft cabins is expected to be significant for personnel such as the pilot and crewmembers. One potential application includes wireless weather for pilots to use. It would allow graphical weather data to be updated directly to the pilot screen. Currently pilots depend on voice messages for updates on weather patterns that are beyond the onboard weather radar system. Cabin crew can utilize wireless networks to upload information updates, and download information to the ground such as the amount of duty-free items needed to be replaced, meal quantities needed for the next flight or maintenance information [5,10].

### **Current Implementations**

Since wireless networks have existed for the past decade, there is already been a move to implement them in aircraft cabins. European Airline Lufthansa has already started trials in their charter planes the Condor; they have recently gained approval to

install a wireless radio connection in a Boeing 747-400 provided it meets special structural criteria. The Scandinavian Airlines Systems (SAS) has already boasted by the spring of 2005 it “will be the first airline in the world to invest exclusively in wireless technology for Internet onboard” [5].

Competition from other international airlines is pushing the Federal Aviation Administration (FAA) to reexamine its position. They are concerned with wireless networks interfering with onboard communications systems. But the tremendous boom in the wireless network industry, with revenue expected to be \$83 million from wireless technology, has led to the FAA predicting that the approval of in-flight systems may occur in another year or two [5].

Implementing a wireless system on airplanes hasn't been tested in the cabin extensively in the United States. Airlines are financially constrained after September 11<sup>th</sup> and physically testing can be done but it is both expensive and time consuming. Another problem is that airplane models vary from company-to-company, type, and year produced. Airline companies often fit internal configurations to their personal specifications. Therefore it is cost prohibitive to physically test each configuration in a commercial fleet.

## **Modeling and Simulation**

Modeling and simulation could be applied to the various airplane classes to produce a general idea of wireless network design and optimum placement of network components. Simple models of the individual aircrafts can be used to examine the effects

of wireless networks in the fuselage. Thus an electromagnetic propagation prediction tool can be used to simulate the environment in an aircraft cabin.

Modeling and simulation is advantageous in many ways; it can decrease the time and cost associated with physical testing while providing quick parameter change on demand. This would provide an erudite method of examining the electromagnetic propagation of the signals.

There are many electromagnetic propagation prediction tools on the market. Wireless Insite by Remcom Inc. will be used to test whether it is an effective and accurate method of simulation of a wireless communication system within aircraft cabins. To verify the effectiveness of Wireless Insite a simulation environment will be created on the basis of an experimental study done by the Embry Riddle Aeronautical University.

## **Objectives**

The objectives of this study are to simulate the power propagation in three types of aircraft fuselages. A comparison will be made between empty and full fuselage to examine the effects of internal components. The propagation model types will also be compared for accuracy to experimental study.

This thesis will be divided into four sections. Chapter Two will cover the background and experimental study associated with the simulation. Chapter Three will touch upon the simulation setup and the work completed. Chapter Four will focus on the results and data analysis of the simulation with Chapter Five offering conclusions of the work completed and suggestions for future work.

## II. BACKGROUND

### WLAN

Wireless Local Area Networks (WLAN) have gained popularity over the past decade. They serve as a data transmission system in a network via radio waves rather than a cable. It is expected that WLAN industry will grow to \$1.6 billion this year. One of the advantages of a WLAN is its relative ease of setup. Access points transmit the signal via antenna to wireless laptops or client cards [5,10].

The Institute of Electrical and Electronic Engineers [IEEE] has set standards under which these systems can operate. Three current standards in use are 802.11a, 802.11b, and 802.11g, (therein will be referred to as 11a, 11b, and 11g, respectively). The standards differ in many ways, which include signal modulation technique, operation frequency, and data rate transfer.

### Signal Modulation

Signal modulation is the method in which the signal is transmitted in a network. In a basic communication system there are three components, the transmitter, the receiver and the transmission channel. The transmitter takes an input signal and modifies the signal to be sent over the transmission channel; for WLAN the transmission channel are radio waves. This modification is the signal modulation. The 802.11 standards modulate the signal by either orthogonal frequency division multiplexing or direct spread spectrum technology [3].

The 802.11a uses orthogonal frequency division multiplexing [OFDM] as its encoding scheme; it was developed for indoor use. OFDM transmits multiple signals

simultaneously over a path. Each of the signals is transmitted with their own distinct frequency range or carrier. The carriers are spaced at particular frequencies, which allow the demodulators to see only that particular signal. OFDM has numerous benefits, which include spectral efficiency, lower multi-path distortion and high data rates. The orthogonality allows the subcarriers to overlap; this has a positive effect on spectral efficiency. The subcarriers are exactly far enough apart from one another to avoid interference. The subcarriers are shown below [3].

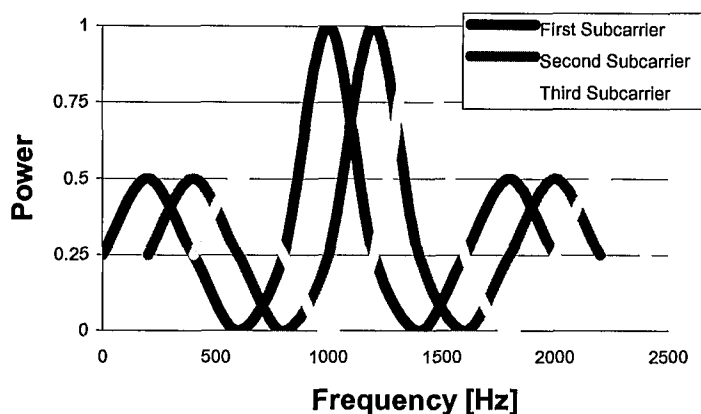


**Figure 1: OFDM efficient use of Bandwidth.**

There are also some drawbacks to OFDM such as large peak to average power ratio, and the issue of multiple versions of the signal. A large peak-to-average-power [PAP] ratio can distort the signal if the transmitter uses a power amplifier to transmit the signal. The peak of the signal can be  $x \cdot (\text{average power})$  where  $x$  is the number of subcarriers. A large peak increases intermodulation distortion [11].

The 802.11b standard uses Direct Spread Spectrum Technology [DSSS]. Originally used by the military for secure wireless transmission it allows the data to be sent over a broad frequency rather than a single frequency. The signal is passed through a spreading function and then is distributed over a band. The signal is easier to detect with

spread spectrum than OFDS. The DSSS uses a redundant bit pattern, called a chip, for each bit to be transmitted. The longer the chip, the more bandwidth required and the better chances of it being recovered by the receiver. One disadvantage of 802.11b is that the frequency band is crowded thus it may be interfered from other networking technologies under some circumstances [3].

## **Operation Frequency and Data Rate Transfer**

The 802.11a provides bandwidth up to 54 Mbps in the 5 GHz band, though realistically the bandwidth is usually about 30 Mbps. The problem with 11a is that since it operates at a higher frequency the 11a signals have a harder time penetrating walls and other objects, thus being more easily obstructed. The average range of the 802.11a signal is much lower than its counterparts, usually ranging from 25 to 100 feet [3].

The 802.11b standard provides a bandwidth of up to 11 Mbps in the 2.4 GHz band. The signal range of 11b is also not easily obstructed. 802.11b is also the most common used standard due to its greater distance range.

The 802.11g standard can be considered a hybrid of 11a and 11b. It provides the same bandwidth as 11a and also uses the OFDM encoding scheme, but it operates in the 2.4 GHz band. It is relatively new compared to the other two standards and is not as popular [9].

## **Signal Propagation Effects**

Signals propagating from any of these standards face problems that wired networks do not. When a signal propagates from the transmitter to the receiver there is a

possibility of multipath effects. The receiver picks up reflected, diffracted, and attenuated copies of the transmitted signal if there is no line of sight path due to surrounding objects. Reflection occurs when a wave meets a boundary and changes directions; diffraction is when the wave bends around the boundary or obstacle [11].

When a signal reflects off an obstruction and then travels to the receiver, the signal is delayed and has traveled a longer distance to reach the receiver. Thus the signal has lost energy from the reflection. The multiple waves that are traveling recombine at the receiver. They can modify the waveform and consequently affect the signal quality at the receiver. Therefore multipath can be dependent on the objects in the WLAN environment, the transmitter-receiver distance, line of sight, and radio technology. Figure 2 depicts a WLAN system in which waves are traveling from two transmitters to two possible receivers. The letter “D” in the diagram represents where the signal has diffracted and “R” represents where the signal has reflected off the surface. A signal can undergo multiple diffractions and reflection before it reaches the receiver [11].

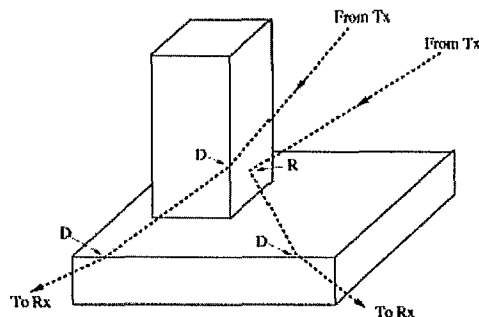


**Figure 2: Example of Diffraction and Reflection of Signals off an Arbitrary Building. [2]**

Diffraction and reflection are going to play a key role when examining the power propagation in the fuselage. When WLAN's are used in an environment, there is desire to have very few obstructions so that line of sight can be maximized. A fuselage is more

crowded than the average environment. It is composed of an aluminum alloy, which will account for some signal reflections. Another factor is the number of people that are in the fuselage. The signal can also decay quite rapidly with distance in this setting. Therefore understanding how electromagnetic waves travel in complex environments has been the focus of many studies [6,11].

## Previous Experimental Study

The study by Embry Riddle Aeronautical University consisted of testing an enterprise grade unit, the Orinoco AP2000, and two units that are intended for SOHO use, the Linksys and NetGear units. Of the three, the Orinoco AP2000 was chosen to conduct the experiment. A WLAN was constructed by using the access points and multiple laptop computers. The parameters of the Orinoco AP2000 are shown in Table 1 [1].

**Table 1: Summary of Access Point Parameters**

Access Points	ORiNOCO AP 2000
Standard	802.11a & 802.11b
Antenna Type	Two Linear Dipole Antennas (11a) Integrated Antenna (11b)
Antenna Gain	5.0 dBi (11a) 2.0dbi (11b)
Output Power	802.11a:17dBm 802.11b: 18dBm
Polarization	Vertical

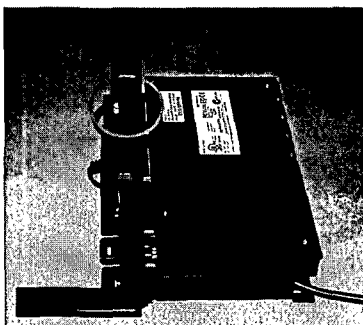


**Figure 3: Orinoco AP2000.**

Figure 3 shows the Orinoco AP2000. The two linear dipole antennas are shown in the rectangles. When operated together they act as an omnidirectional antenna. The integrated antenna is shown circled. The dual operation of the system allows for the tests to be conducted for both standards [1,13].

The testing consisted of one laptop connected to the access point [AP] and it acts as a server while the other laptops with client cards act as receivers. AirMagnet Wireless Network Analyzer was used to help collect data such as data rate and received power. The second parameter is the one of most interest, since it is assumed that an aircraft fuselage acts as a leaky reverberation chamber. This would influence the propagation of radio signals [1].

### **Limitation in Experimental Study**

Four aircrafts were tested by Embry-Riddle; these include the Boeing 747-400, 767-300, 777-200, and the Airbus A320. The actual aircraft test environment differed greatly from ideal conditions. Personnel were noted to be moving around in addition to doors being ajar, and cabin furnishing being disassembled. The cabin furnishing being disassembled only factored into B767-300 and B747-400 environments. The seat arrangements and door status played varying roles in power readings during testing. Specifically in the B747-400 maintenance was being performed in the first class area and the doors one [right side] and five [left side] were open and door four [left side] was ajar. For the B767-300 rows 21-22 were removed and stacked on rows 24-25, in addition door one [right side] was open. The Boeing 777-200 had all doors open for ventilation. In

most cases the airplanes were powered down, in instances that they were powered up, it was noted that there was little and no differences in measurements [1].

## Experimental Setup

The data was collected and was referenced to the LOPA (Layout of Passenger Accommodations) and then mapped as station numbers. Station numbers are the number of inches from a specified point labeled in the aircraft fuselage. The B767 had inconsistent station numbers, but the conversion from station numbers to inches is further described in the experimental study. The transmitters were situated in various locations in the fuselages. More specifically they were placed as follows. The B747 AP was located on the back of seat 6D, B777 AP was located between the footrest of seats 1E and 1D, and the B767 AP was located on the back of seat 1E. For the A320 the AP was located in the back of the fuselage. Figure 4 shows how the AP and receivers was placed in the fuselage. [1]



(a)



(b)

**Figure 4: Experimental Setup.**  
**(a) Access Point (b) Receiver**

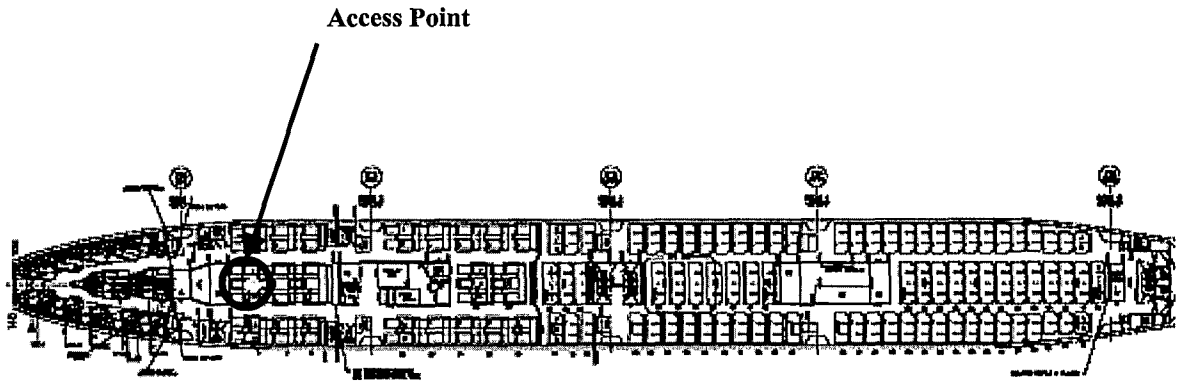


Figure 5: Seat Layout of Boeing 747 with AP location.

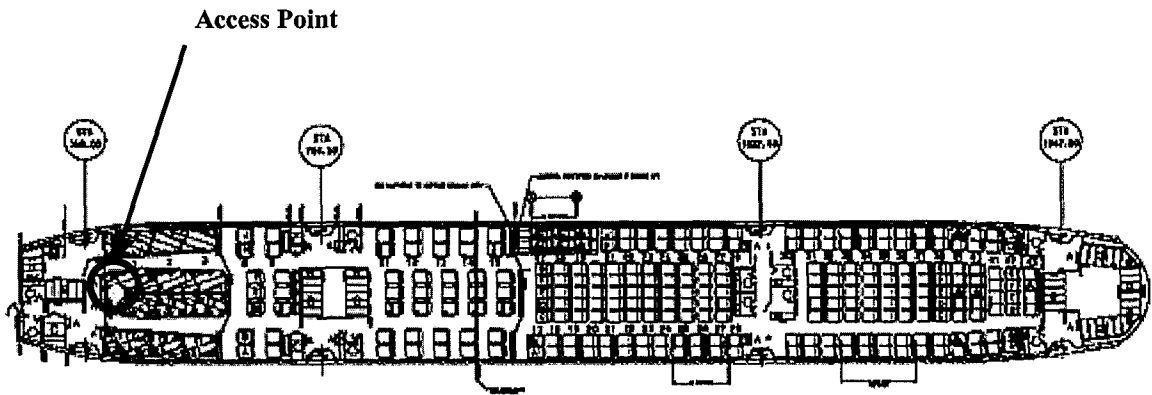


Figure 6: Seat Layout of Boeing 777 with AP location.

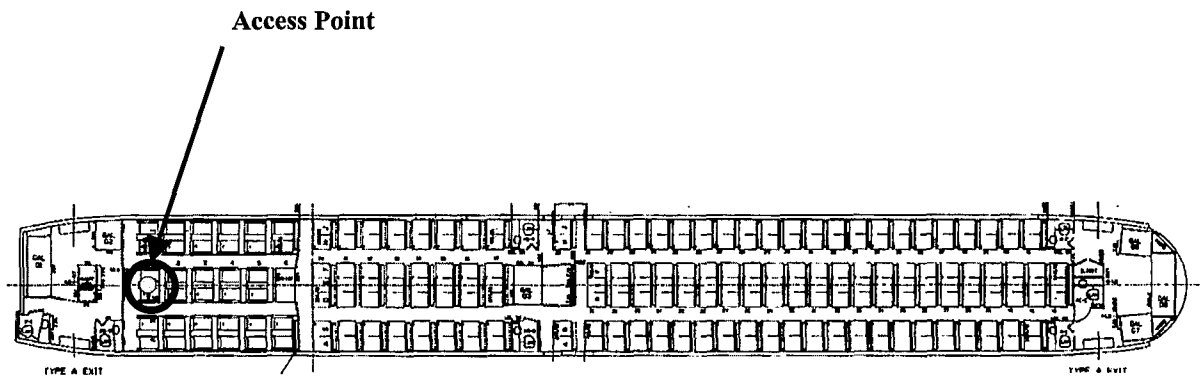
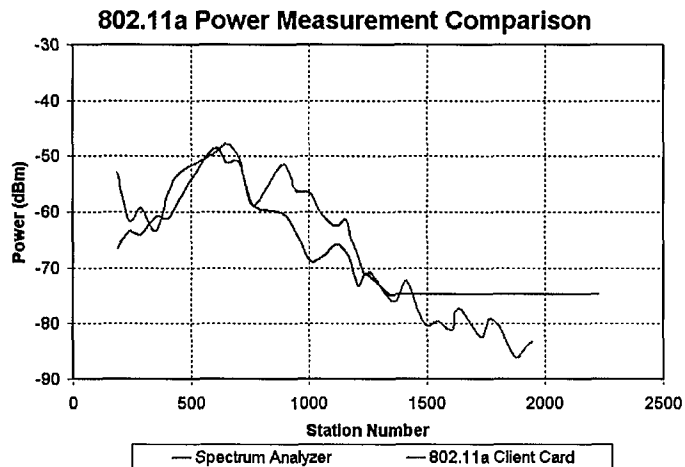
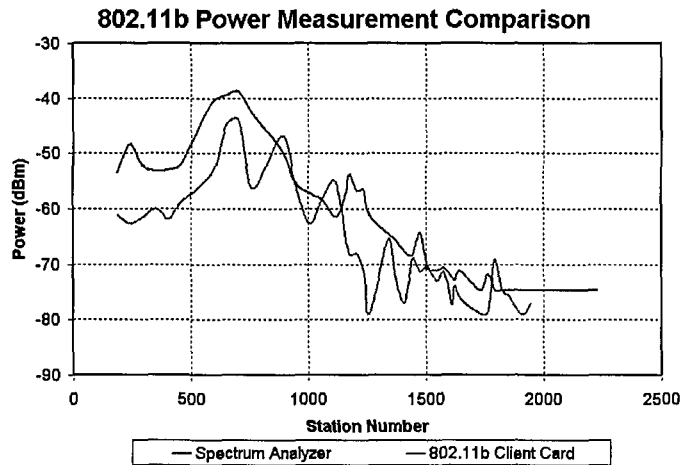


Figure 7: Seat Layout of Boeing 767 with AP location.

## Experimental Results

RF power measurements were collected with a spectrum analyzer and the client card. The power measurement with these two instruments also varied. The spectrum analyzer measures instantaneous power at each discrete frequency whereas the client card uses spread spectrum technology to determine the total power. The spectrum analyzer antenna was also uncalibrated. This will account from some differences between the readings. A comparison between the spectrum analyzer and the client card power was recorded to note any significant differences. Figure 8 below shows the results of the comparison of the spectrum analyzer and the client card in the experimental study. At certain stations the RF power reading varied much as 10 dBm.[1]





**Figure 8: RF Power Reading for Spectrum Analyzer and Client Card.**

The following results were obtained from the experimental study. Figure 9 is the RF power obtained from the B747. The RF power peaks at the location of the AP at station 610. It is also noted that the power then declines in either direction of the AP. The 802.11b has a stronger signal further down the fuselage as compared to 802.11a. The RF power propagation is also shown in Figures 10 and 11 with the same general trend noted for both planes. [1]

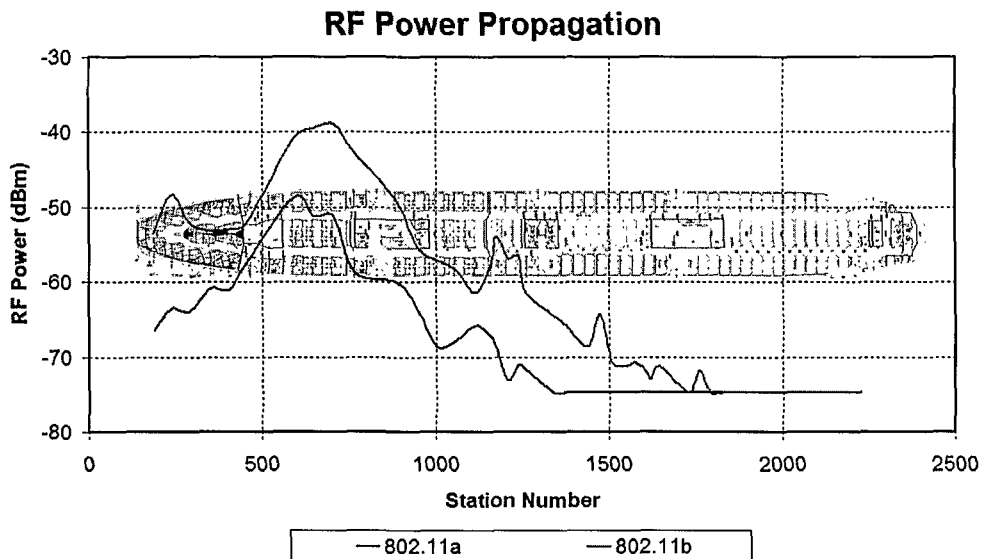


**Figure 9: Experimental Result of RF Power Propagation of B747.**

### RF Power Propagation

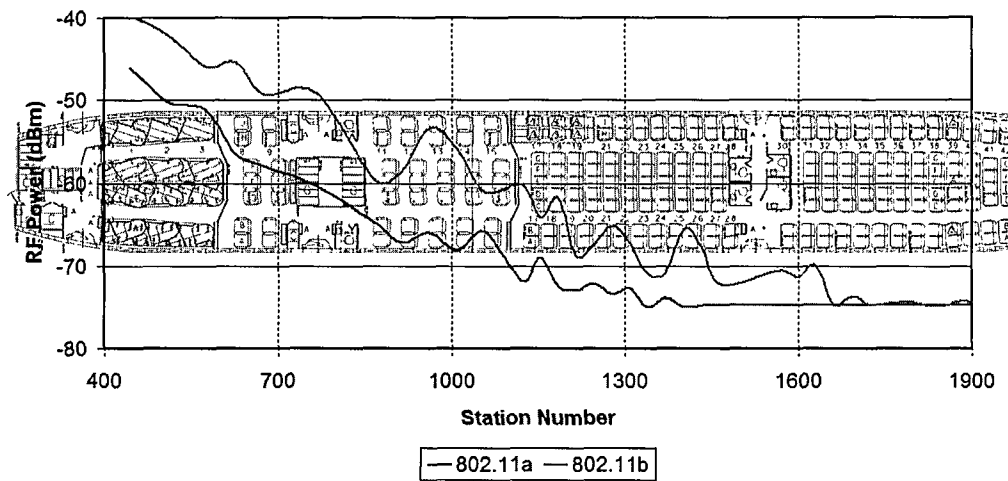


**Figure 10: Experimental Result of RF Power Propagation of B777.**

### RF Power Propagation

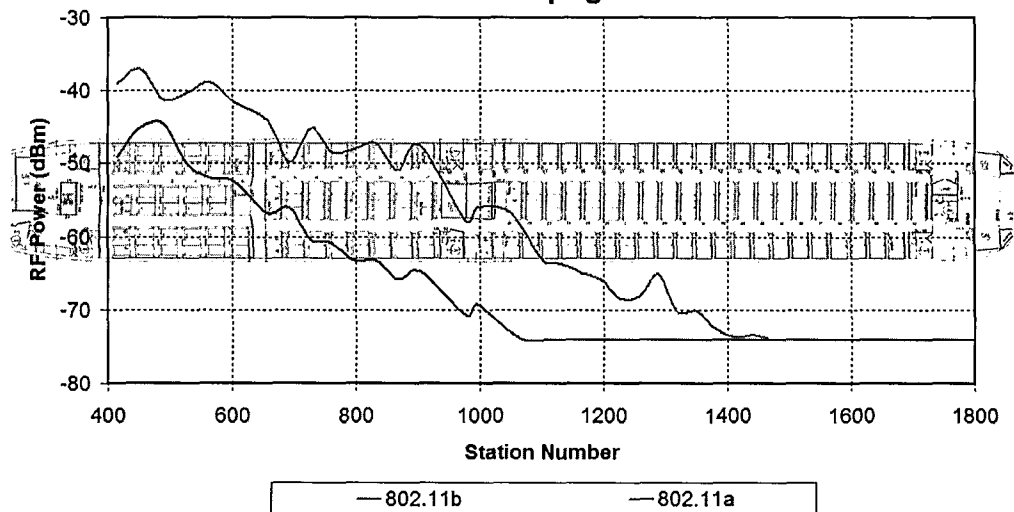


**Figure 11: Experimental Result of RF Power Propagation of B767.**

In Figures 9, 10, and 11, the 802.11b standard has more RF power than the 802.11a standard over distance.

## Electromagnetic Modeling

There are many available codes for use in electromagnetic modeling. Numerical techniques such as Method of Moments and Finite Element often find it difficult to solve

for electromagnetic propagation in a complicated geometry and use very high memory and CPU processing times. The Finite Difference Time Domain [FDTD] method is more suitable to the stated application. [7]

FDTD uses Maxwell's time dependent curl equations show below in Equation 1. The space and time derivatives are calculated in central difference equation form. The area modeled is represented as two grids [Yee's lattice]; one grid is for electric field calculation and the other for the magnetic field. The electric field and magnetic field are alternatively computed. For example the Electric field at time  $t$  is used to calculate the magnetic field at time  $t + \tau$  where,  $\tau$  is the time increment. [7]

The FDTD also allows for each section of the lattice to be assigned  $\mu, \epsilon$ , and  $\sigma$  which describe the parameters of the media. [7]

$$\nabla \times \mathbf{E} = -\mu \frac{\partial \mathbf{H}}{\partial t}$$

$$\nabla \times \mathbf{H} = \sigma \mathbf{E} + \epsilon \frac{\partial \mathbf{E}}{\partial t}$$

Equation 1: Maxwell's Time Dependent Curl Equations [7]

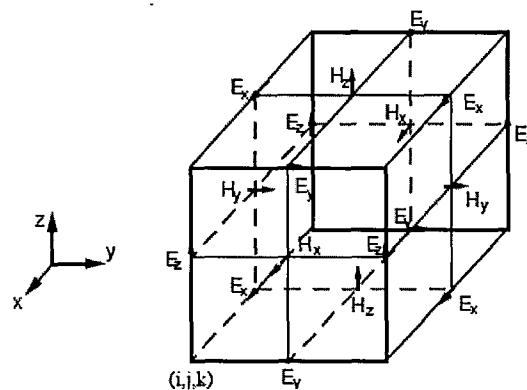


Figure 12: Yee's Lattice[7].

Another approach to examine electromagnetic wave propagation can be to create an electromagnetic code from first principles. The problem lies in the time it takes to create and debug such a code. Thus it was not feasible to create a personalized code.

Modeling software that uses FDTD seems ideal to create and test the fuselage model. Remcom utilizes the FDTD method for its electromagnetic propagation prediction software, Wireless Insite.

### III. SIMULATION

The foundation of the simulation highly depends on the accuracy put forth in recreating the environment. Wireless Insite (WI) is electromagnetic wave propagation prediction software created by Remcom; they use various ray-tracing models as a method of calculation. As mentioned previously, the program uses the Finite-Difference Time-Domain technique [FDTD]. The program is mainly used to predict how signal strength is affected by other parameters in the system such as material properties and shape. Wireless Insite has many benefits including a friendly graphical user interface, propagation over complex terrains, speed, and importation of various file formats. The system requirements are shown in Table 2 [2].

**Table 2: System Requirements for Wireless Insite [2]**

<b>Suggested</b>	<b>Actual</b>
Pentium III	Pentium 4
800 MHz	1.19 GHz
Space needed varies on application	6GB
256 MB of memory	512 MB of memory

#### **Propagation Methods**

WI also provides various propagation methods for the user. Three different methods of propagation were considered for simulation (Urban Canyon, Fast 3D & Full 3D). All three methods were used to predict data. Two of the three methods use approximations to produce data; the third method is expected to be the most accurate (Full 3D), but takes longer to run. Three methods were used for multiple reasons. First, our model of the fuselage system fits the requirements of the three systems. Secondly, it is uncertain which

method can give the most accurate results based on statement one. Lastly, there is a time constraint. It has to be determined whether the approximations made by the model are then adequate for our system. It must be decided if the approximations made by the methods are adequate for our geometries. Only Full 3D is recommended for indoor use. But since the cabin has a unique shape, the indoor method may not be the most accurate [2].

The propagation methods use the shooting and bouncing ray method (SBR). SBR uses geometrical optics to trace the rays. Numerous rays are shot at an object, and then their movement traced according to geometrical optics. When the SBR paths have been traced, a path is recorded [2].

### **Urban Canyon Model**

The first model is the Urban Canyon Model (UCM). It is used when transmitters and receivers are close to the ground in height as compared to the height of other objects. The UCM model uses the shooting and bouncing ray method (SBR) to determine the propagation paths of the transmitters. The ray tracing method uses SBR for horizontal plane and an image method for ground reflections. Since the UCM employs mostly 2D approximations, it assumes that if the heights of other objects around the transmitter and receiver are high, then the ray paths that are diffracted off the top of the objects are negligible compared to the rays that are bouncing between objects. The run time is significantly decreased due to this factor and multiple assumptions. The first assumption is that path length is larger than the receiver and transmitter height difference. This statement allows the UCM to neglect using the multiple reflection and diffraction coefficients. The second assumption made is that vertically polarized components are

almost perpendicular to the plane of propagation and that horizontal components are parallel to the plane. The depolarization of the field is ignored with this assumption. The electric field for each path is calculated with the use of the Uniform Theory of Diffraction [2].

**Table 3: Urban Canyon Model Capabilities [2]**

Maximum reflections	Unlimited
Maximum transmissions	N/A
Maximum diffractions	3
Environment	Urban
Indoor	N/A
Objects	N/A
Range	Usually 1km
Antenna Height	Lower than surrounding objects
Antenna Type	All
Ray Tracing	SBR for horizontal plane and Image Method for ground reflection
Minimum Frequency	100MHz
Maximum Frequency	Dependent on Application

Data for Urban Canyon was collected but it was concluded that the results produced did not fit the scope of the study.

### **Fast 3D Urban Model**

Fast 3D Urban Model (FUM) is the second model tested. This model uses the same method described above but in addition it also takes into account the tops of low lying objects around the transmitter and receivers. The FUM does not use a full 3D trace; Fast 3D means that the vertical components of some objects are considered in the

calculations. FUM incorporates the heights of other objects when making calculations. Basically it is used if there are many objects of varying heights that could possibly have ray paths that affect the calculations. To account for the effects, SBR and multiple image methods in 3D geometry are used. The SBR is used for calculation in the horizontal plane; image method is used for ground reflection and ray path with less than 2 interactions. SBR main purpose is to find the paths of the ray. The program then calculates whether the rays have diffracted, passed over, or intersected a boundary object. Depending on the situation above, paths are constructed and the most probable is obtained. Since, FUM incorporates the heights of other objects when making calculations. It is generally used if there are many objects of varying heights that could possibly have ray paths to affect the calculations [2].

For the FUM to be acceptable, two assumptions must be made. The first assumption is that the distance that the path is shifted vertically is small compared to the path length. This will be valid when the horizontal distance between the transmitter and receiver is greater than the vertical distance. The second assumption made is that shape of an object is not intricate. Since the vertical plane calculation is simplified, a complex shaped would take more paths, which would not be accounted for [2].

**Table 4: Fast 3D Model Capabilities [2]**

Maximum reflections	Unlimited
Maximum transmissions	N/A
Maximum diffractions	3
Environment	Urban
Indoor	N/A
Objects	N/A
Range	Usually 1km

Antenna Height	All
Antenna Type	All
Ray Tracing	SBR for horizontal plane and Image Method for ground reflection and for ray paths with 2 or less interactions
Minimum Frequency	100 MHz
Maximum Frequency	Dependent on Application

### Full 3D Model

The final model used is the Full 3D Method (FM). Of the three models, FM is recommended for indoor simulation and places no constraint on the object shape. It is the only model that allows for transmission through surfaces. Thus it is most applicable for indoor environments. The FM combines SBR and MI ray tracing. MI is used when a path has three or fewer interactions. Paths with more than three interactions are found with SBR method. The thorough use of both methods produces a 3D model that takes into account many parameters. It is expected to deliver the most accurate results of the three models. The run time of this particular model is proportional to the number of transmissions ( $N_T$ ) and the number of reflections ( $N_R$ ). The number of diffractions also plays a role in run time. When zero diffraction are requested, the run time is equal to the number of faces in the object. When one diffraction is requested the run time is approximately the number of faces squared. More than one diffraction does not alter run time significant since the program has a limitation on the coplanar edges of an object. On average the run time for the Full 3D method ranged from one to six hours. [2]

**Table 5: Full 3D Model Capabilities [2]**

Maximum reflections	Unlimited for non-diffracted paths, 2 reflections with diffractions
Maximum transmissions	Unlimited
Maximum diffractions	3 (SBR) 2 (Eigenray)
Environment	all
Indoor	all
Objects	all
Range	Dependent on application
Antenna Height	All
Antenna Type	All
Ray Tracing	SBR or Eigenray
Minimum Frequency	100 MHz
Maximum Frequency	Dependent on Application

## Fuselage Models

### Rectangular Models

The most efficient way to build the cabin model was to import data exchange files (.dxf), which were created in an AUTOCAD capable program. Two different cabin representations (a rectangular prism and a half-cylinder) were initially used in the simulation, and no internal cabin details such as windows, galleys, doors, seats or overhead cargo bins were included. The rectangular prism had the same cabin cross sectional area as the three aircraft cabins. All cabins had two models except for the B747-400. This cabin has two levels and the experimental measurements were collected on the lower level. The 747-400 cabin geometry was a rectangular shape with a front-end taper. A second floor was also added since it will couple energy from the power propagation. These simple cabin models were created to provide some general insight into the software validity and the absorption and reflection of internal components.

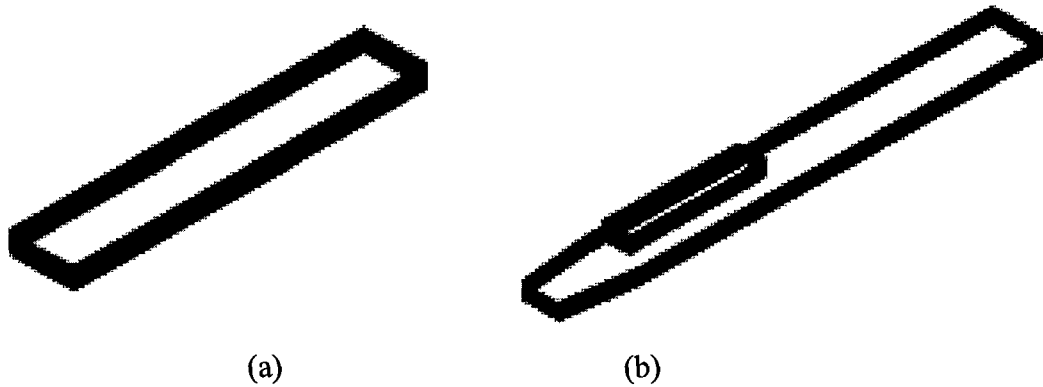


**Figure 13: Rectangular Models (a) Generic Boeing Model (b) Boeing 747.**



**Figure 14: Cylindrical Models.**

The main idea behind creating these rectangles was to observe whether the creation of a rectangular fuselage was adequate representation of the cylindrical fuselage. When the power levels of the two models were compared, it was noted that the rectangular model was not as accurate as the cylindrical model and there were inconsistencies with the accuracy of the data. Thus it was concluded that a cylindrical model should be used for further simulation purposes. The data for the empty rectangular models are shown below for the Boeing 777 and 767. It was noted previously that the

Boeing 747 already has a rectangular shape. The Mean Average Error (MAE) and Root Mean Square Error (RMSE) are shown for each plane and defined in Equation 18.

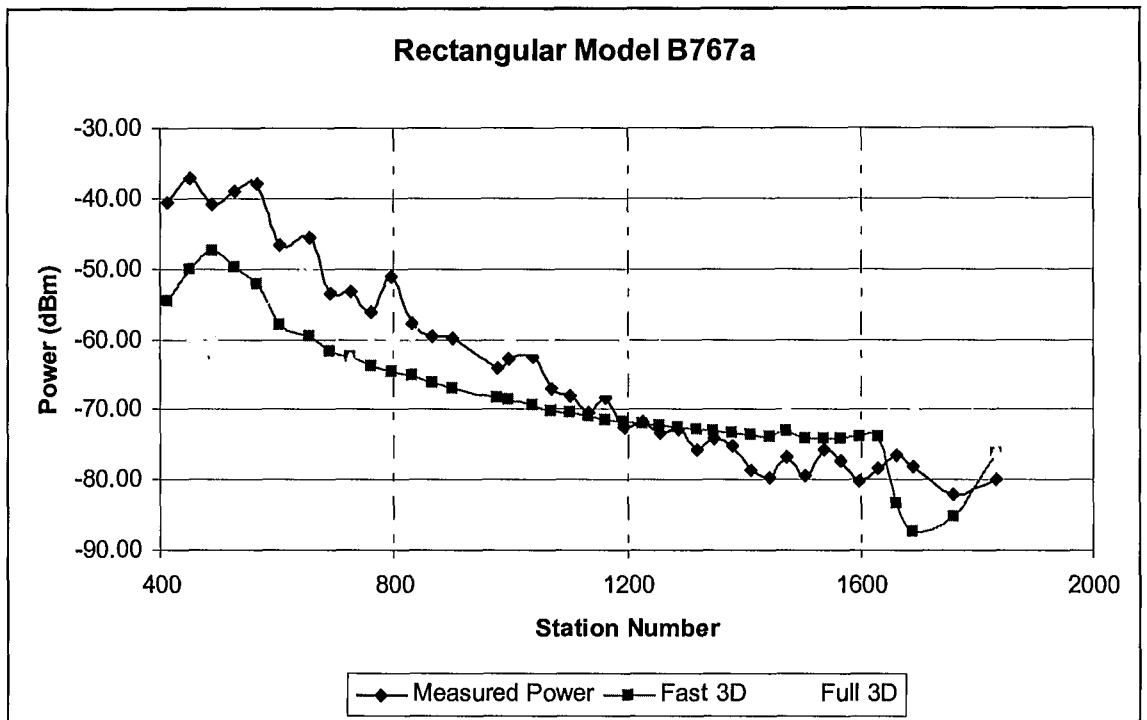


**Figure 15: Rectangular Model B767a.**

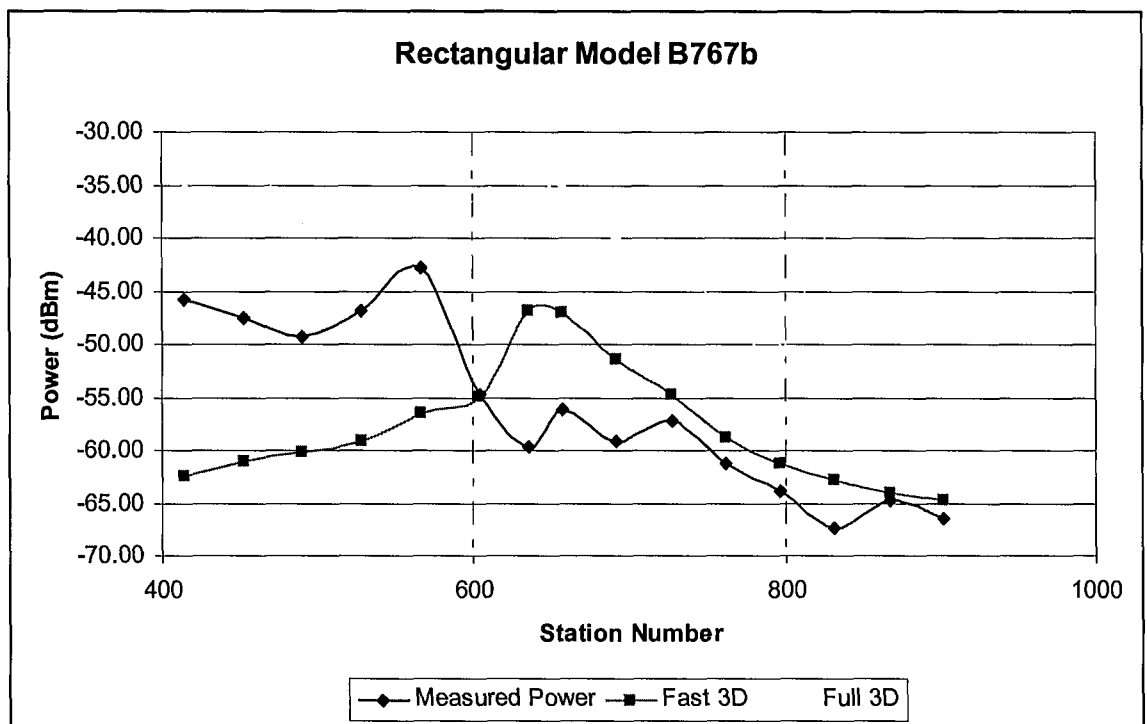


**Figure 16: Rectangular Model B767b.**

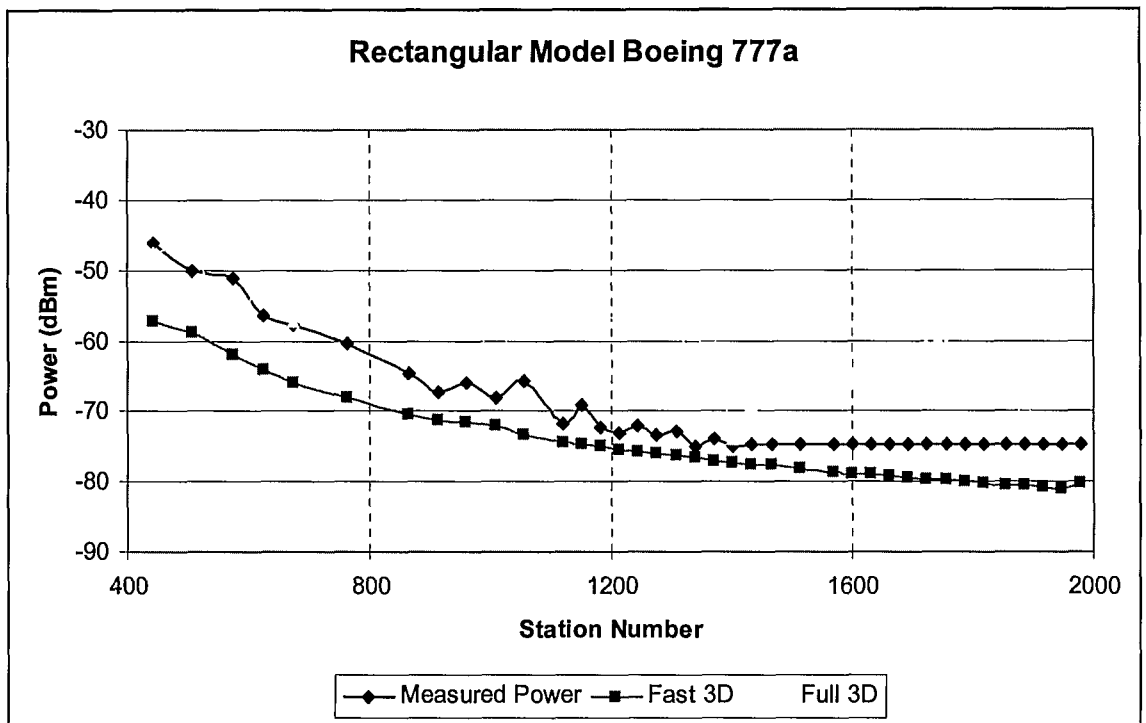


**Figure 17: Rectangular Model B777a.**

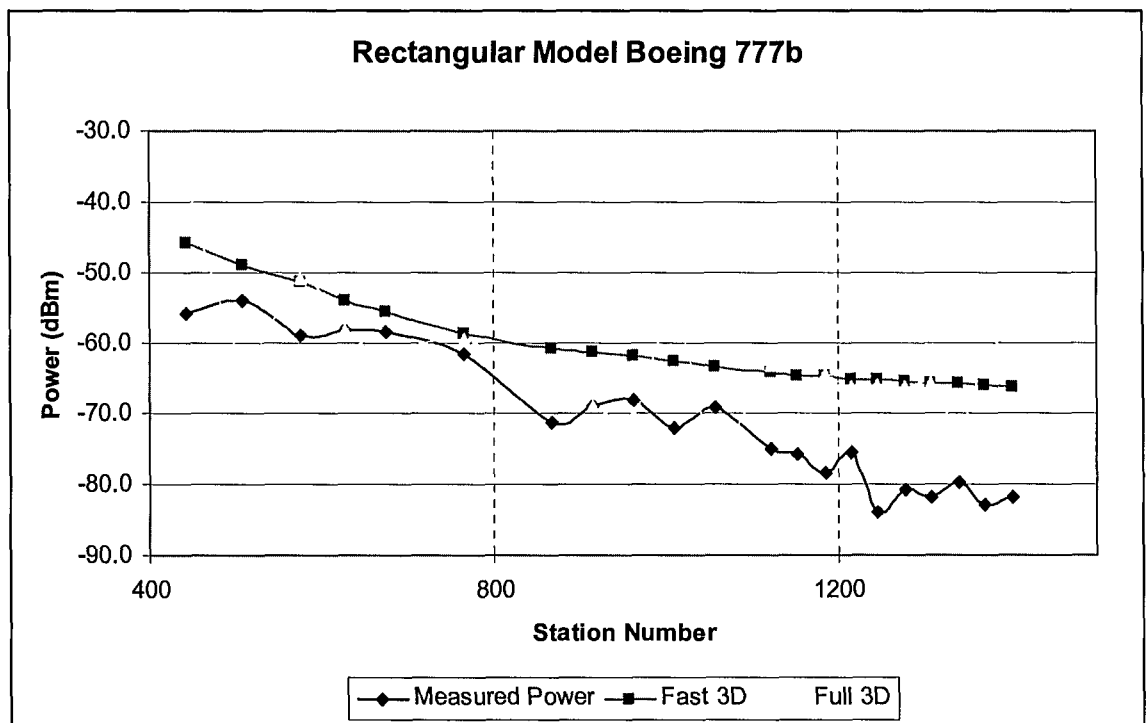


**Figure 18: Rectangular Model B777ab.**

**Table 6: MAE and RMSE Data for Fast 3D**

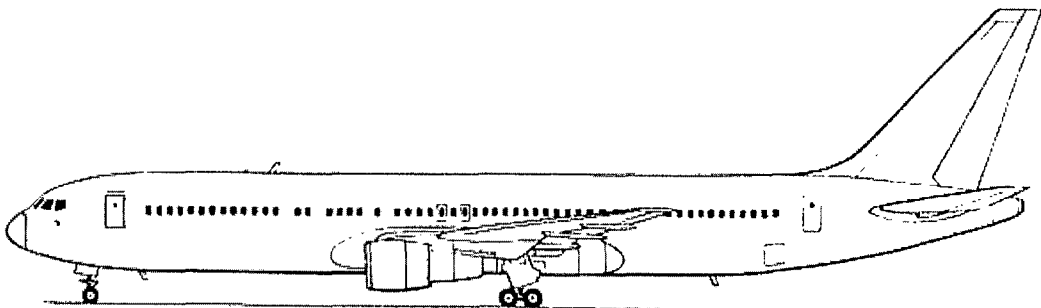
	MAE	RMSE	
Rectangular Fuselage	5.903	7.183	B767a
Rectangular Fuselage	7.458	9.214	B767b
Rectangular Fuselage	5.0345	5.505	B777a
Rectangular Fuselage	10.206	11.186	B777b

**Table 7: MAE and RMSE Data for Full 3D**

	MAE	RMSE	
Rectangular Fuselage	9.429	10.883	B767a
Rectangular Fuselage	17.582	11.681	B767b
Rectangular Fuselage	9.831	10.867	B777a
Rectangular Fuselage	10.405	12.529	B777b

## Cylindrical Models

The new models were created in Solidworks®. Solidworks provides an easier venue for creating the models rather than AutoCAD. There were two models created for the B747, B767, and B777. The first was a simple empty cylindrical model. The second model was a completed fuselage that included seats, doors, windows, galleys and bathrooms. The window and door dimensions were obtained from a CAD drawing provided by Boeing. Each window and door was measured and created to the exact dimensions that were noted in the Boeing files [12].

**Figure 19: Boeing CAD Drawing used for Dimensioning.**

The seats were laid out by using various seating arrangements. The seat pitch and width was an important factor to consider. For the first class, business class, and coach sections the seat pitch and width varied.

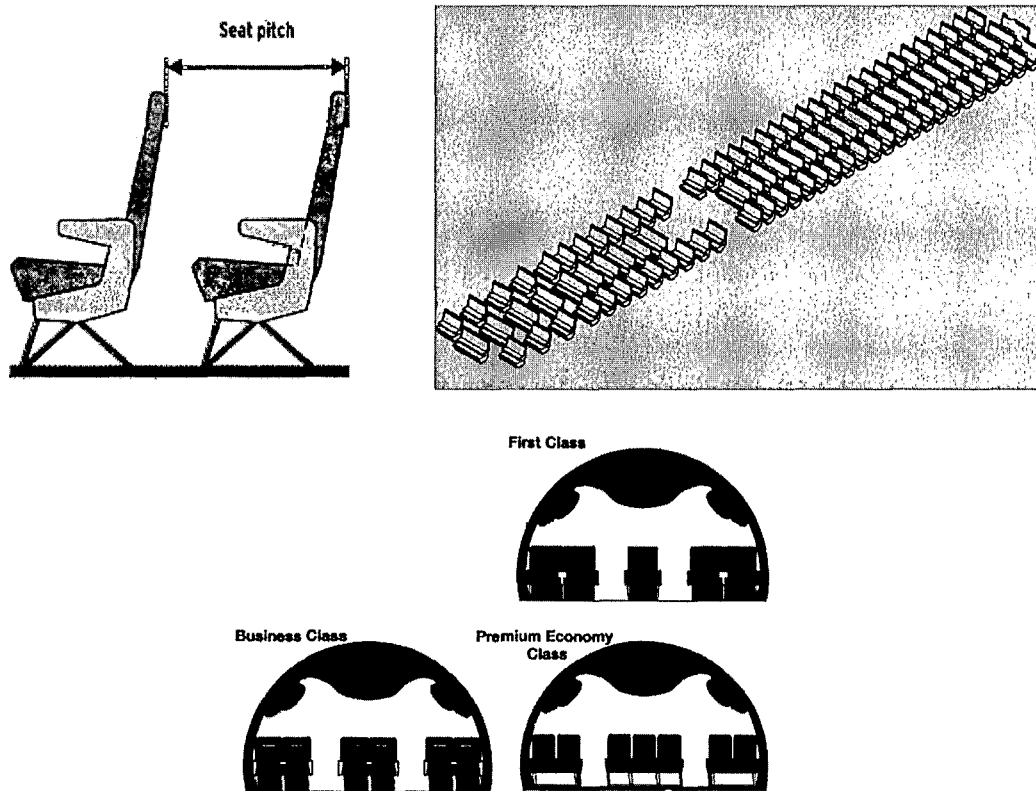


**Figure 20: Seat Arrangements.**

The purpose of creating two models was to study the effects of the internal components on the power propagation. The models were then imported as STL files into Wireless Insite. For simulation purposes it was assumed that the fuselage metal was a Perfect Electrical Conductor (PEC). The fuselages when assigned as a PEC will reflect all energy, and the transmission coefficient is zero. The two parameters assigned to the PEC are thickness and roughness. Roughness is defined as the standard deviation of the

surface height with regards to the mean height in meters. The seats were assigned as a foam material [an absorber]; the windows were assigned as a thick glass that was available in the material database.

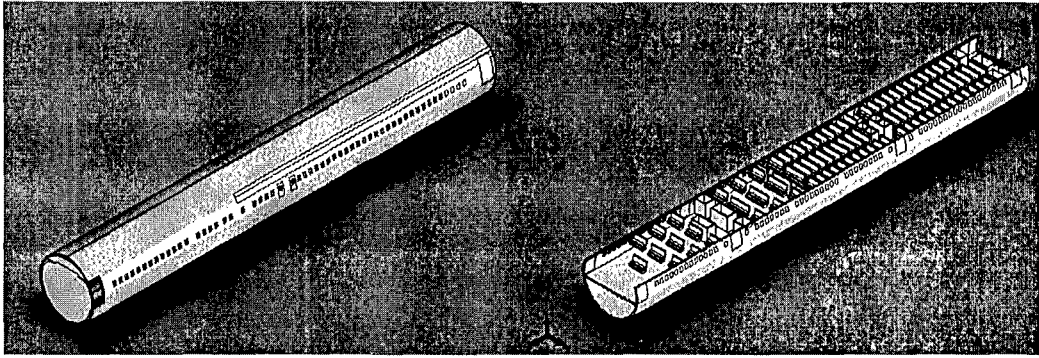


**Figure 21: Boeing 767 Model depicted in Solidworks ®.**

## Importation

One problem encountered with the models was the level of detail. WI can only handle a certain number of faces for each of the structures imported. The models created had over 100,000 faces and then were reduced to approximately 32,000 faces which is the maximum number of faces that Wireless Insite can handle. Another Remcom product XGTD was used to import the STL files and then they were reduced. For example instead of the cylinder being represented as a 300-sided polygon, it was reduced to be a 100-sided polygon. The fuselages were then exported as .obj files that are used by WI. Examples of the models when imported into Wireless Insite are shown in Figure 16.

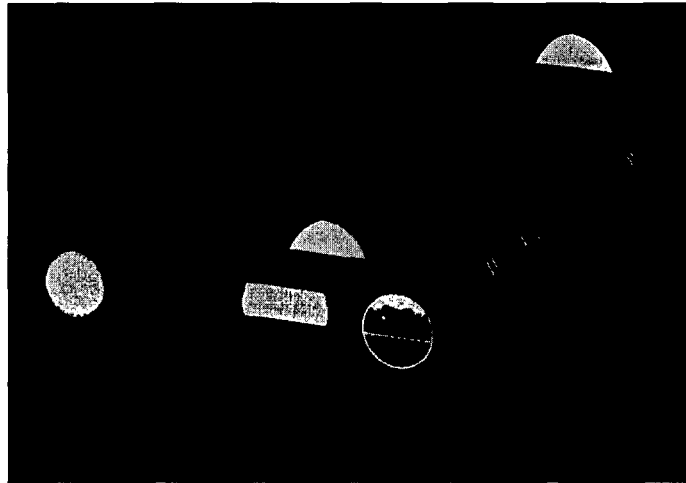
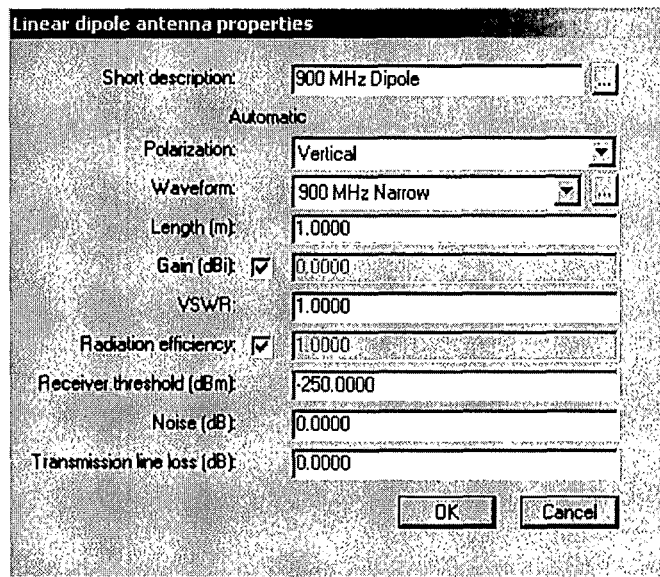


Figure 22: Fuselage Models in Wireless Insite.

### **Antennas, Receivers, & Transmitters**

Four different antennas were needed to model the 11a and 11b standards. Each antenna is associated with a waveform. For the transmitters, an omnidirectional antenna was used for 11a standard and an integrated antenna for 11b; each antenna has individualized waveform, antenna length, gain, polarization, and transmission line loss. The WI database provided the antenna basics for the transmitter. WI also generates the antenna patterns (visual depiction of the E-plane and the H-plane on different axes).



**Figure 23: Example of WI screenshot of Antenna Properties.**

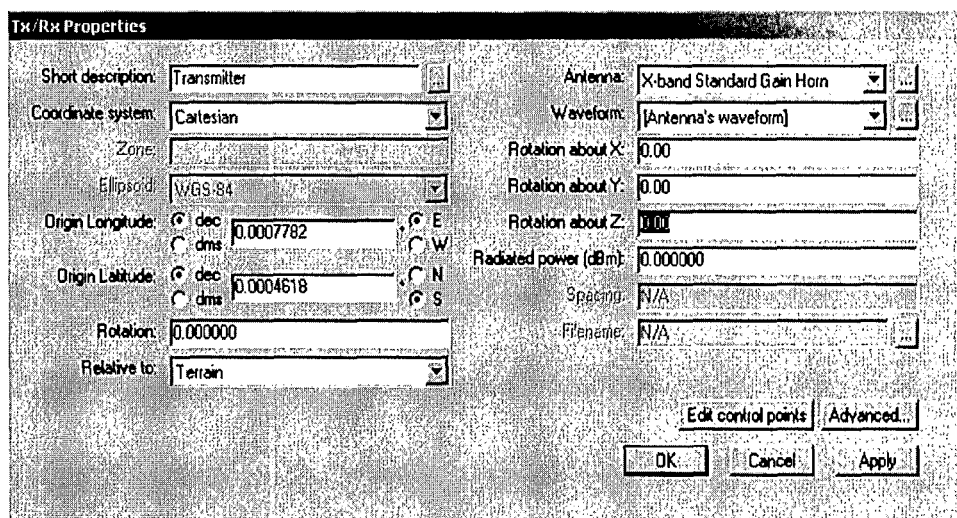


**Figure 24: WI Screenshot of Basic Transmitter Properties.**

The receiver antennas were not generated by the WI database since they are integrated antennas. An antenna format file that designates gain and polarization was created from the antenna pattern of the receiver that was obtained from the FCC Website. The antenna was then imported and assigned to the receiver. Again each system antenna had the same specifications. The waveform for each antenna was also created.

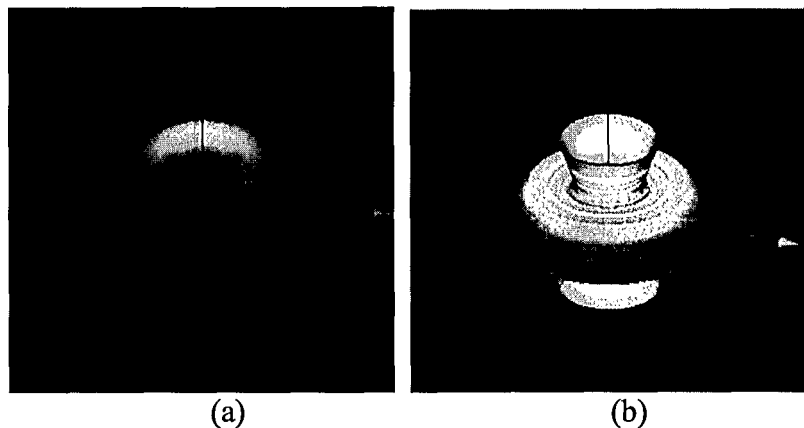


**Figure 25: 3D Antenna Pattern (a) Omnidirectional Antenna  
(b) Client Card Receiver Antenna [2].**

Transmitter and receiver placement was the next step. To determine the accuracy of the data compared to experimental results, it was important to place the transmitters and receivers in the same location and orientation as the experimental setup. Transmitters needed the following properties to operate: coordinate system, elevation type, rotation, waveform, antenna type, radiated power, and rotation about each plane in the xyz system. The height, rotation about the axis, and orientation differed for each airplane. Receivers were easier to place. The receivers were laid as a strip on the left portion of the fuselage. The receiver ran from the transmitter to the end of the fuselage. Ideally the receiver can be placed on the airplane tray or the seat. Figure 26 depicts the transmitter and receiver layout from the front of the cabin. Figure 27 shows the receiver layout in the experiment study as compared to the simulation. The variation on color indicates the power received for each receiver. This will be discussed in the upcoming chapter.

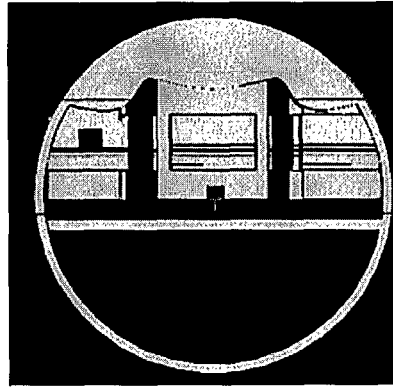


**Figure 26: WI Depiction of Fuselage with Transmitter and Receivers.**

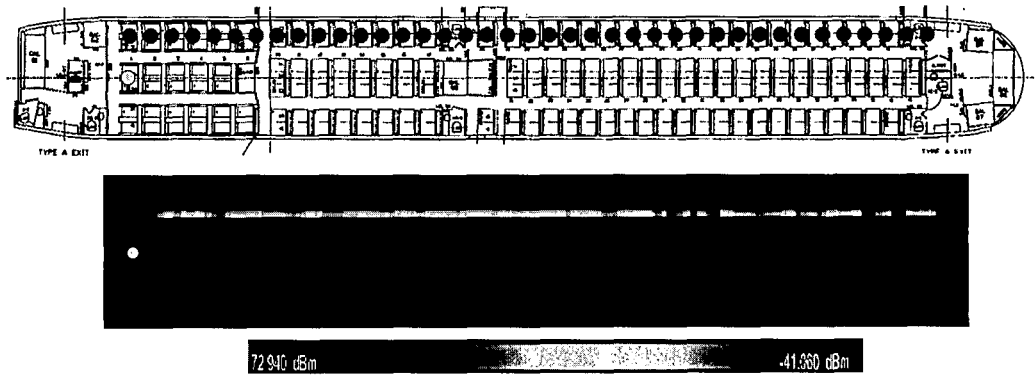


**Figure 27: Receiver Layout Compared to Experimental Study.**

## ELECTRIC FIELD CALCULATIONS

The spherical coordinate system used in Wireless Insite for reference in the following equations is shown below.

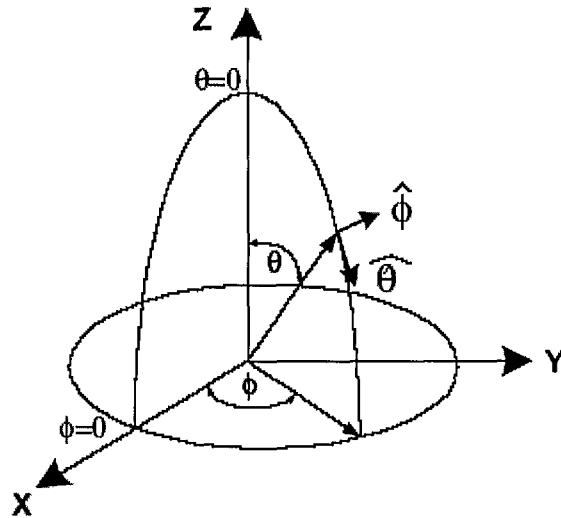


Figure 28: Wireless Insite Spherical Coordinate System [2].

### Urban Canyon Method:

The electric field in the far zone of the transmitting antenna is first found. The equation below is used with line-of-sight (LOS) rays to the receiver. In free space the electric field [with direction of  $\phi$  and  $\theta$  and distance of  $r$ ] is defined as follows:

$$\mathbf{E}(r, \theta, \phi) = \left( A_{\theta}(\theta, \phi) \hat{\mathbf{e}}_{\theta} + A_{\phi}(\theta, \phi) \hat{\mathbf{e}}_{\phi} \right) \frac{e^{-j\beta r}}{r}$$

Equation 2: Electric Field in Free Space [2]

with

$$A_{\theta}(\theta, \phi) = \sqrt{\frac{P_T \eta_0}{2\pi}} g_{\theta}(\theta, \phi)$$

$$A_{\phi}(\theta, \phi) = \sqrt{\frac{P_T \eta_0}{2\pi}} g_{\phi}(\theta, \phi)$$

$$g_{\theta}(\theta, \phi) = |G_{\theta}(\theta, \phi)|^{1/2} e^{j\psi_{\theta}}$$

The symbol  $G_{\theta}(\theta, \phi)$  represents the  $\theta$  component of the gain of the transmitting antenna. The letter  $\Psi_{\theta}$  is the relative phase of the  $\theta$  component of the far zone electric field. The same definition holds true for the  $\phi$  component. The bandwidth,  $\beta$ , is defined as a function of frequency and speed of light below [2].

$$\beta = \omega/c$$

The symbol  $P_T$  represents the time-averaged power radiated from transmitter with  $r$  being the field point distance from transmitter.

A ray reflected  $N$  times is the next scenario considered. The electric field in the  $\theta$  and  $\phi$  direction is defined in Equations 3 and 4 respectively.  $R_n^{\perp}$  is the reflection coefficient of the  $n^{\text{th}}$  reflection for the plane perpendicular to the plane of incidence and  $R_n^{\parallel}$  is the reflection coefficient for the component parallel to the plane of incidence.

$$E_{\theta} = A_{\theta}(\theta, \phi) \frac{e^{-j\beta r_{TR}}}{r_{TR}} \prod_{n=1}^N R_n^{\perp}$$

**Equation 3: Electric Field in theta Direction [2]**

$$E_{\phi} = A_{\phi}(\theta, \phi) \frac{e^{-j\beta r_{TR}}}{r_{TR}} \prod_{n=1}^N R_n^{\parallel}$$

**Equation 4: Electric Field in phi direction [2]**

Thus the total field with this specific path is defined in Equation 5 . Usually one component is greater than the other. When the antenna is vertically polarized then  $E_\theta$  is greater than  $E_\phi$ . If the antenna is horizontally polarized then  $E_\phi$  is typically greater in value than  $E_\theta$ .

$$\mathbf{E} = E_\theta \hat{\mathbf{e}}_\theta + E_\phi \hat{\mathbf{e}}_\phi$$

**Equation 5: Total Electric Field [2]**

The complex electric field from ground reflection is shown in Equation 6. In this equation  $R_G^\parallel$  is the ground reflection coefficient for the field component parallel to the plane of incidence.

$$E_\theta = A_\theta(\theta, \phi) \frac{e^{-j\beta r_{TR}}}{r_{TR}} R_G^\parallel \prod_{n=1}^N R_n^\perp$$

**Equation 6: Complex Electric Field from Ground Reflection [2]**

For diffracted rays the complex electric field is expressed in Equations 7 and 8 for the  $\theta$  and  $\phi$  direction. In these equations, N is the number of reflections before diffractions and M is the number of reflections after initial diffraction until it reaches the receiver. The distance between the transmitter and diffraction point is  $r_{TD}$  and  $r_{DR}$  is the distance from the diffraction point to the receiver.  $D_s$  and  $D_h$  are the diffraction coefficient for the component parallel to the diffracting edge and for the component perpendicular to the diffracting edge respectively.

$$E_\theta = A_\theta(\theta, \phi) \frac{e^{-j\beta r_{TR}}}{r_{TD}} \prod_{n=1}^N R_n^\perp \cdot D_s \cdot \sqrt{\frac{r_{TD}}{r_{DR}(r_{TD} + r_{DR})}} \cdot \prod_{m=1}^M R_m^\perp$$

**Equation 7 [2]**

$$E_{\phi} = A_{\phi}(\theta, \phi) \frac{e^{-j\beta r_{TR}}}{r_{TD}} \prod_{n=1}^N R_n^{\parallel} \cdot D_h \cdot \sqrt{\frac{r_{TD}}{r_{DR}(r_{TD} + r_{DR})}} \cdot \prod_{m=1}^M R_m^{\parallel}$$

**Equation 8 [2]**

The complex electric field for ground reflection for the  $\theta$  component is expressed in Equation 9. The  $\phi$  component has an analogous definition.

$$E_{\theta} = A_{\theta}(\theta, \phi) \frac{e^{-j\beta r_{TR}}}{r_{TD}} \cdot R_G^{\parallel} \cdot \prod_{n=1}^N R_n^{\perp} \cdot D_s \cdot \sqrt{\frac{r_{TD}}{r_{DR}(r_{TD} + r_{DR})}} \cdot \prod_{m=1}^M R_m^{\perp}$$

**Equation 9[2]**

For multiple diffractions, Equation 10 is used. In this equation, N is the number of reflection before the first diffraction, Q is the number of reflections between the diffractions and M is number of reflections after the second diffraction. Additional variables include:  $r_{T1}$  which is the distance from transmitter to first diffraction point,  $r_{12}$  is the distance between the two diffraction points,  $r_{2R}$  is the distance from second diffraction point to receiver, and  $D_s$  (1) and  $D_s$  (2) are the diffraction coefficients for the first and second diffractions.

$$E_{\theta} = A_{\theta}(\theta, \phi) \frac{e^{-j\beta r_{TR}}}{r_{T1}} \prod_{n=1}^N R_n^{\perp} \cdot D_s(1) \cdot \sqrt{\frac{r_{T1}}{r_{12}(r_{T1} + r_{12})}} \cdot \prod_{q=1}^Q R_q^{\perp} \cdot D_s(2) \cdot \sqrt{\frac{r_{T1} + r_{12}}{r_{2R}(r_{T1} + r_{12} + r_{2R})}} \cdot \prod_{m=1}^M R_m^{\perp}$$

**Equation 10 [2]**

### **Fast 3D and Full 3D Method:**

In free space the electric field [with direction of  $\phi$  and  $\theta$  and distance of  $r$ ] is defined as follows:

$$E(r, \theta, \phi) = \left( A_\theta(\theta, \phi) \hat{e}_\theta + A_\phi(\theta, \phi) \hat{e}_\phi \right) \frac{e^{-j\beta r}}{r}$$

Equation 11

With

$$A_\theta(\theta, \phi) = \sqrt{\frac{P_T \eta_0}{2\pi}} g_\theta(\theta, \phi)$$

$$A_\phi(\theta, \phi) = \sqrt{\frac{P_T \eta_0}{2\pi}} g_\phi(\theta, \phi)$$

$$g_\theta(\theta, \phi) = |G_\theta(\theta, \phi)|^{1/2} e^{j\psi_\theta}$$

$G_\theta(\theta, \phi)$  is the  $\theta$  component of the gain of the transmitting antenna.  $\Psi_\theta$  is the relative phase of the  $\theta$  component of the far zone electric field. The same definition holds true for the  $\phi$  component. Bandwidth,  $\beta$ , is defined as a function of frequency and speed of light.

$$\beta = \omega/c$$

$P_T$  is the time-averaged power radiated from transmitter with  $r$  being the field point distance from transmitter.

The electric field amplitude calculation is more complex than that of Urban Canyon's calculation. The incident electric field when reflected is not always parallel or perpendicular to the plane of incidence. The field is a combination of both. The reflected field is defined by the components of the reflected electric field that is parallel and perpendicular to the reflected plane in Equation 12. The variables used are defined as  $E_{\parallel}^r$  is the electric field of the reflected wave parallel to plane of incidence,  $E_{\perp}^r$  is the electric field of the reflected wave perpendicular to the plane of incidence,  $R_{\parallel}$  is the

reflection coefficient of the plane parallel to the plane of incidence, and  $R_{\perp}$  is the reflection coefficient of the plane perpendicular to the plane of incidence.

$$\begin{pmatrix} E_{\parallel}^r \\ E_{\perp}^r \end{pmatrix} = \begin{pmatrix} R_{\parallel} & 0 \\ 0 & R_{\perp} \end{pmatrix} \begin{pmatrix} E_{\parallel}^i \\ E_{\perp}^i \end{pmatrix}$$

**Equation 12 [2]**

Where,

$$E_{\perp}^i = \hat{e}_{\perp} \cdot E^i$$

$$E_{\parallel}^i = \hat{e}_{\parallel} \cdot E^i$$

$$\hat{e}_{\parallel} = \mathbf{k} \times \hat{e}_{\perp} / |\mathbf{k} \times \hat{e}_{\perp}|$$

$$\hat{e}_{\perp} = \mathbf{k} \times \hat{n} / |\mathbf{k} \times \hat{n}|$$

$$\hat{e}'_{\parallel} = \mathbf{k}' \times \hat{e}_{\perp} / |\mathbf{k}' \times \hat{e}_{\perp}|$$

The vector  $\mathbf{k}$  is the direction of propagation of incident field and  $\mathbf{k}'$  is the direction of propagation of the reflected field.

Therefore the reflected field is defined in Equation 13.

$$E^r = \hat{e}'_{\parallel} \cdot E_{\parallel}^r + \hat{e}_{\perp} \cdot E_{\perp}^r$$

**Equation 13: Electric Field for Single Reflection [2]**

For diffractions the equations become more complex due to the three dimensions considered for the Fast 3D and Full 3D propagation methods. Previously with the Urban Canyon method the fields are normal to diffracting edges, but for the other propagation methods the fields can be polarized in any direction. Using the generalization used by Luebbers and Burnside the diffracted fields are represented with an “edge-fixed

coordinate system.” The coordinate systems are further explained in the papers by Luebbbers and Burnside.

## Power Calculation

Power calculations differed in each environment. The received power is defined as the total power received by the receiver antenna. It is measured in units of dBm, which is a measure of decibels relative to 1mW of power (0 dBm = 1mW).

The time averaged received power for Wireless Insite ( $P_R$ ) is calculated by the following relationships. The received power is calculated by summing the individual power in the electric field without the phase information in Equation 14.

$$P_R = \sum_{i=1}^{N_p} P_i$$

**Equation 14: Received Power [2]**

In Equation 14,  $N_p$  = number of paths,  $P_i$  = time averaged power (in watts) of the  $i$ th path. Time-averaged power is calculated as:

$$P_i = \frac{\lambda^2 \beta}{8\pi^2 \eta_0} \left| E_{\theta,i} g_{\theta}(\theta_i, \phi_i) + E_{\phi,i} g_{\phi}(\theta_i, \phi_i) \right|^2$$

**Equation 15: Time Averaged Power [2]**

In Equation 15,  $\lambda$  = wavelength,  $\eta_0$  = impedance of free space,  $\beta$  = overlap of frequency spectrum of the transmitted waveform.  $E_{\theta,i}$  and  $E_{\phi,i}$  are the  $\theta$ - and  $\phi$ - components of the electric field of the  $i$ th path at the receiver path.  $\theta_i$  and  $\phi_i$  define the arrival direction,

$g_\theta(\theta_i, \phi_i) = |G_\theta(\theta_i, \phi_i)|^{1/2} e^{i\psi}$  where  $G_\theta$  is the  $\theta$ -component of the receiver antenna gain and  $\psi$  the relative phase of the  $\theta$ -component of the far zone electric field. This is similarly defined for  $g_\phi$ .  $\beta$  is defined as

$$\beta = \frac{\int_{f_T - B_T/2}^{f_T + B_T/2} S_T(f) S_R(f) df}{\int_{f_T - B_T/2}^{f_T + B_T/2} S_R(f) df}$$

**Equation 16: Overlap of Frequency Spectrum of the Transmitted Waveform**

where  $f_T$  and  $B_T$  are the center frequency and bandwidth of the transmitted waveform,  $S_T(f)$  is the frequency spectrum of the transmitted waveform and  $S_R(f)$  is that for the received waveform [2].

## IV. ANALYSIS OF DATA

The data are divided into three sections. All the data will be presented in comparison with the experimental study mentioned in Chapter II. The first section will compare the effect of internal components on power propagation; it is further divided by propagation method. The more accurate system will then be examined for the second section of the results. A comparison between the Fast 3D and the Full 3D propagation methods and the most accurate will be determined. The final section will examine the predicted power propagation between the 802.11a and 802.11b standards. The 11a and 11b standards will be compared with relation to power strength along the fuselage. The graph for all the planes will be displayed with a discussion following each subsection.

A small correction factor was included in the data because the receiver threshold was approximately -75 dBm for the client card where it was about -80 dBm for the receivers in the program. Also there are data points where the loss due to material property was not accounted for; it is added to the data set. All the data will be presented in comparison with the experimental mentioned in Chapter II.

The Mean Absolute Error (MAE) and Root Mean-Squared Error (RMSE) were calculated for the predicted power in comparison to the measured power. The MAE will determine the average difference between measured and predicted power. The RMSE will help determine whether the difference in the MAE is significantly greater than the average prediction. If the RMSE is much greater than the MAE this will indicate that predicted error is greater than the average predicted error. The equations for the MAE and RMSE are presented as Equation 17 and Equation 18. Where  $P_M$  is the measured power,  $P_P$  is the predicted power, and  $N$  is the number of data points collected.

$$MAE = \frac{\sum |P_M - P_P|}{N}$$

**Equation 17: Mean Absolute Error**

$$RMSE = \sqrt{\frac{\sum (P_M - P_P)^2}{N}}$$

**Equation 18: Root Mean Square Error**

**Internal Component Analysis: Empty Fuselage versus Completed Fuselage**

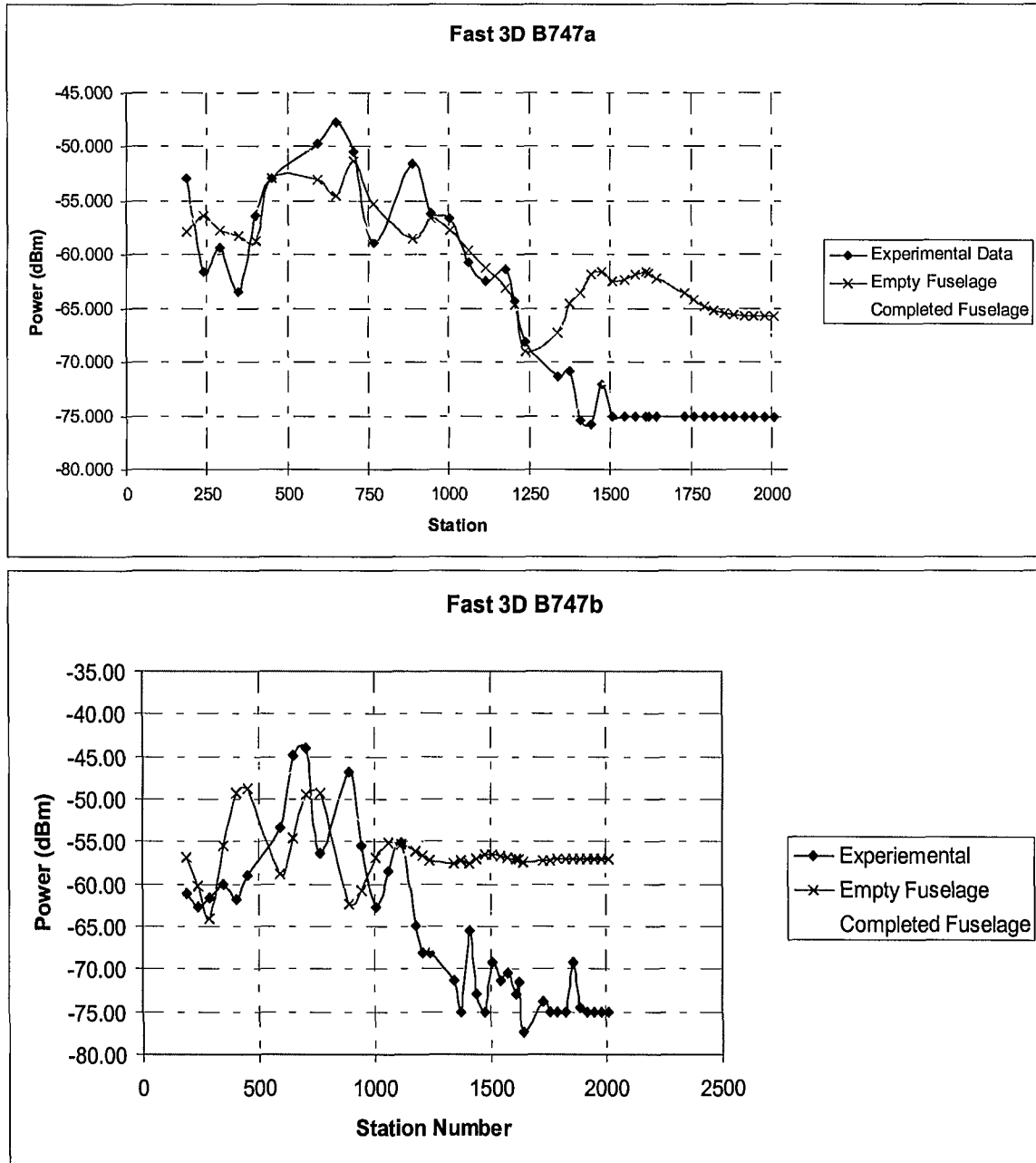


**Figure 29: B747 (a) 802.11a Standard (b) 802.11b Standard.**

**Table 8: MAE and RMSE Comparison for B747 using Fast 3D Method**

	MAE	RMSE	
Empty Fuselage	6.966	8.344	B747a
Completed Fuselage	4.379	5.034	
Empty Fuselage	11.848	13.115	B747b
Completed Fuselage	10.027	11.100	
	Experimental Data		

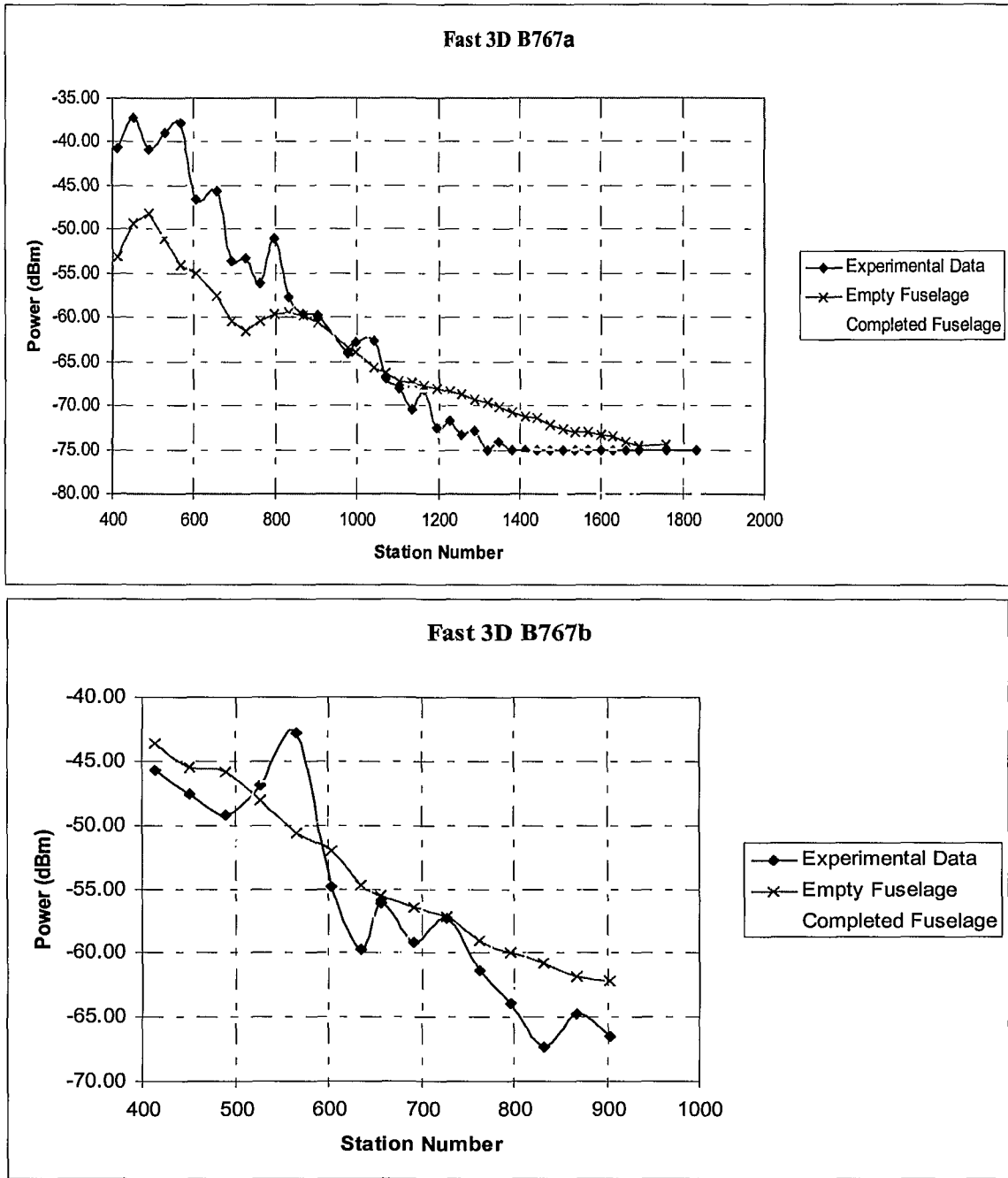


**Figure 30: B767 (a) 802.11a Standard (b) 802.11b Standard.**

**Table 9: MAE and RMSE Comparison for B747 using Fast 3D Method**

	MAE	RMSE	
Empty Fuselage	4.331	5.903	B767a
Completed Fuselage	4.318	5.992	
Empty Fuselage	3.170	3.765	B767b
Completed Fuselage	5.564	6.488	
Experimental Data			

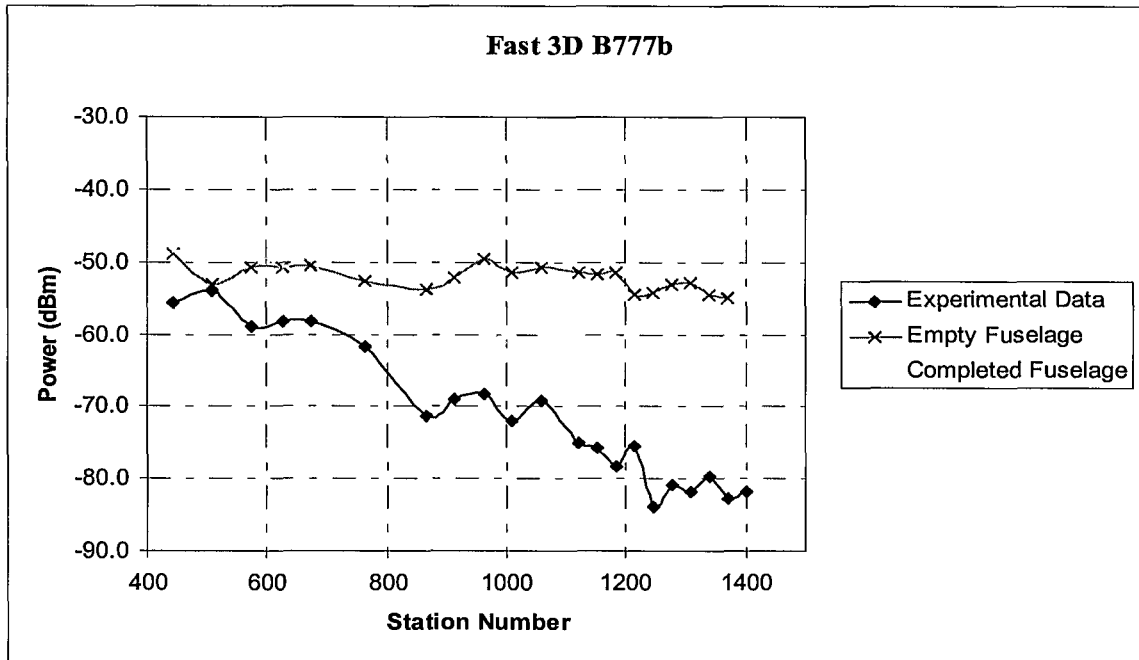
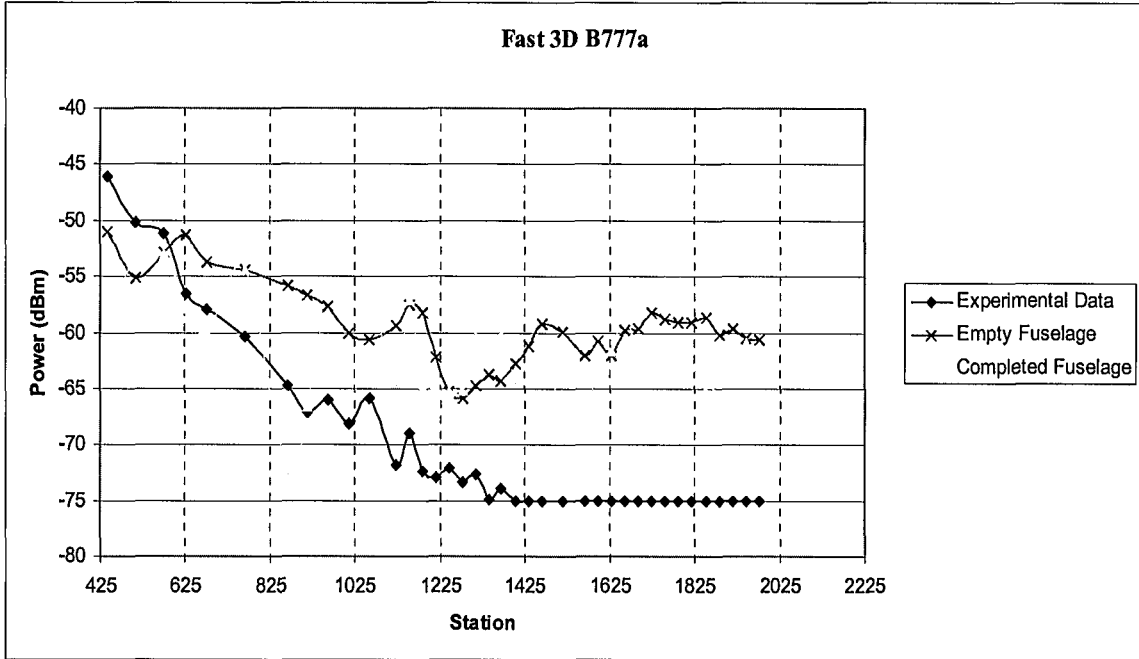


**Figure 31: B777 (a) 802.11a Standard (b) 802.11b Standard.**

**Table 10: MAE and RMSE Comparison for B777 using Fast 3D Method**

	MAE	RMSE	
Empty Fuselage	11.246	12.000	B777a
Completed Fuselage	9.866	10.636	
Empty Fuselage	16.406	17.748	B777b
Completed Fuselage	9.524	10.160	
Experimental Data			

## **Analysis:**

The B747, B767, B777 completed cabins have a lower mean average error than the empty cabins. The signal for the completed fuselage also attenuates with the experimental results. The empty cabin has a higher overall received power than the completed cabin. This can be attributed to the signal undergoing decay through absorption for the completed cabin. The attenuation of the power is more significant in the completed due to the interior components. Yet in the simulation the signal for the completed fuselage does not decay as steadily as expected. This can be attributed to the cabin material properties. Recall that the fuselage was assumed to be a perfect electrical conductor; this could increase reflection, and in turn increase the signal power.

For the B747 the peak power received is noted to be around station 610. This is expected since that is the location of the AP. The power level decays from that point on along the fuselage. At around station 1400 there is a significant drop in the power. This can be attributed to the galley wall. It can be assumed that the signal is weakened when it comes to that point in fuselage.

The B767 the MAE and the RMSE values are closer in value than for the other airplanes. The completed cabin in the both simulations has a lower power level in the front of the cabin as compared to the experimental data. At station 575 to 625 there is another drop in the power for both the experimental data and the completed fuselage; there is a wall at that location and thus can attribute to signal decay. The B777 show little to no decay in power for the empty fuselage; the power difference is no more than 10 dBm. Again, this can be attributed to the lack of internal components.

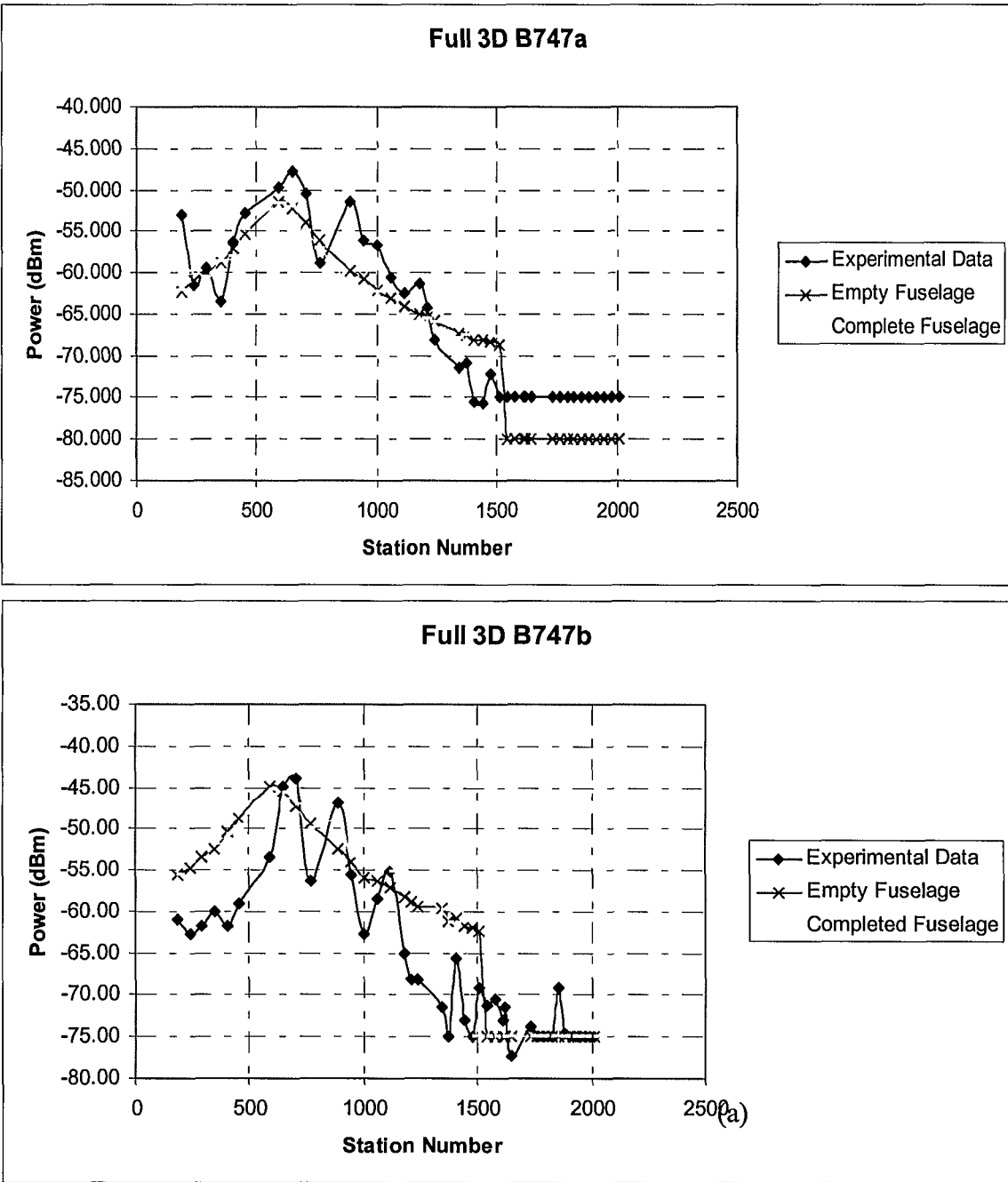


Figure 32: B747 (a) 802.11a Standard (b) 802.11b Standard.

Table 11: MAE and RMSE Comparison for B747 using Full 3D Method

	MAE	RMSE	
Empty Fuselage	4.300	4.744	B747a
Completed Fuselage	4.200	4.748	
Empty Fuselage	5.083	6.546	B747b
Completed Fuselage	4.778	6.355	
Experimental Data			

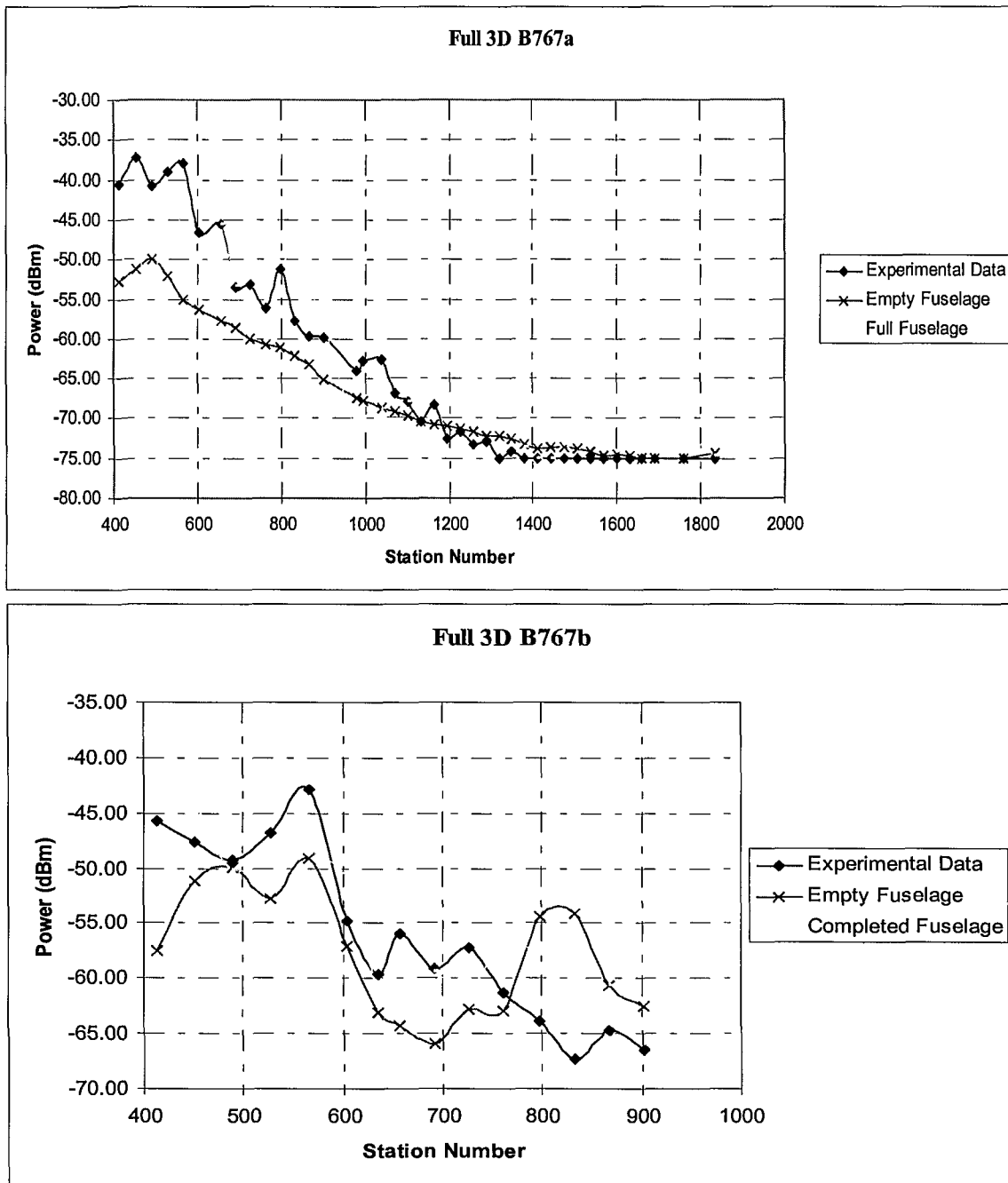


Figure 33: B767 (a) 802.11a Standard (b) 802.11b Standard.

Table 12: MAE and RMSE Comparison for B767 using Full 3D Method

	MAE	RMSE	
Empty Fuselage	4.154	6.124	B767a
Completed Fuselage	4.054	5.272	
Empty Fuselage	5.796	6.771	B767b
Completed Fuselage	4.186	5.055	
	Experimental Data		

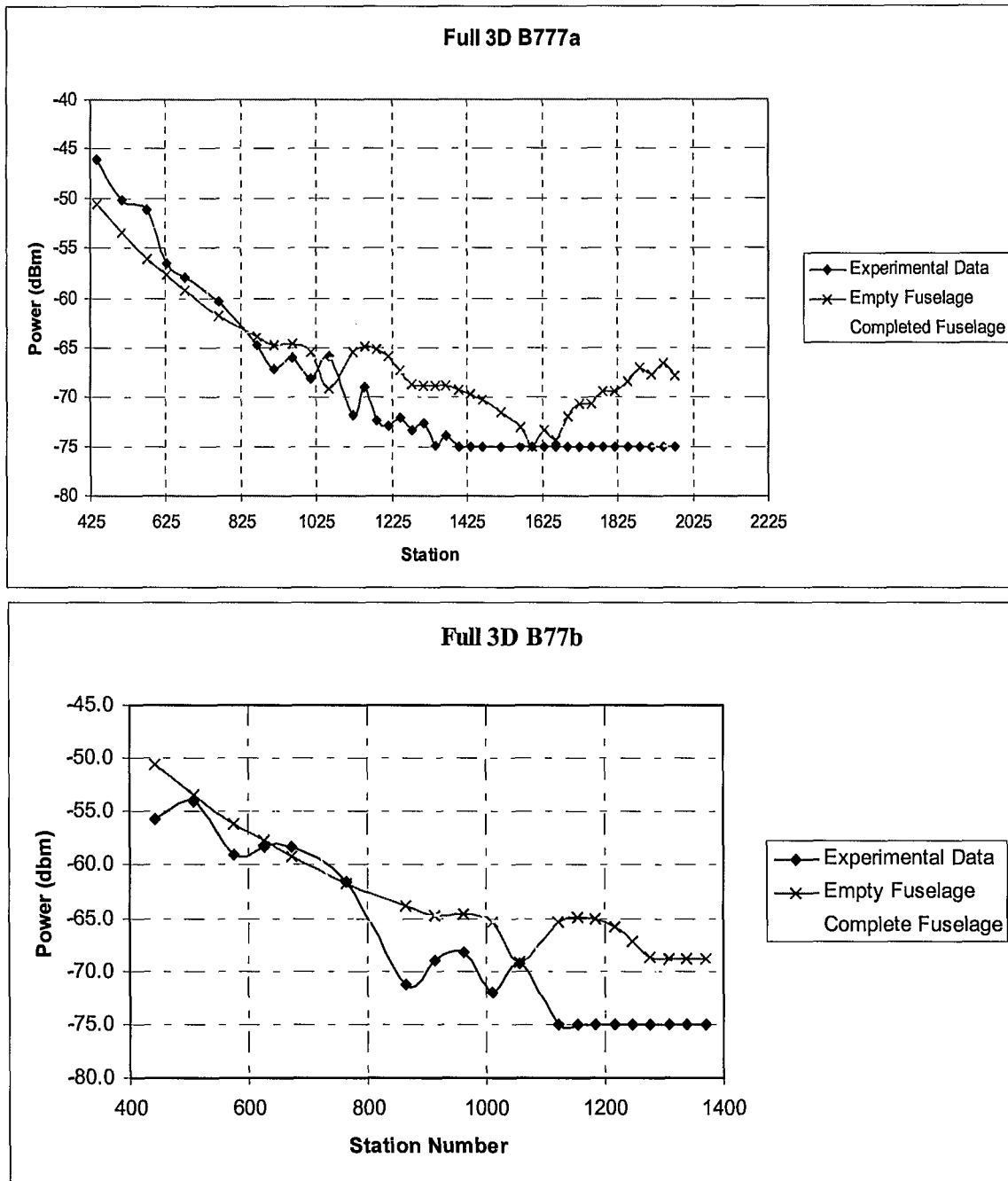


Figure 34: B777 (a) 802.11a Standard (b) 802.11b Standard.

Table 13: MAE and RMSE Comparison for B777a using Full 3D Method

	MAE	RMSE	
Empty Fuselage	4.234	4.785	B777a
Completed Fuselage	3.126	3.844	
Empty Fuselage	5.182	6.150	B777b
Completed Fuselage	4.228	4.632	
Experimental Data			

**Analysis:**

Overall, the completed cabin has a lower error than that of the empty cabin. The difference in the values of the MAE and RMSE is very little when using the Full3D trace. The peak power for the B747 is located where the AP is positioned. There is a sharp drop at station 1500 for all four plots. It is interesting to observe that the power obtained for the B747 does not differ much between an empty and completed cabin. In fact the attenuation is not as great as previously noted. This could be due to the shape of the B747. Recall that the B747 is rectangular in nature due to the second level; the shape may effect the wave propagation. For all three airplanes, the empty fuselage has a smooth decay, which is expected with the absence of internal components. The internal components are effecting the power propagation and the propagation paths, which are evident in the Fast 3D section. The next section will compare how the propagation method affects a completed fuselage.

### Propagation Model Analysis: Fast 3D Method versus Full 3D Method

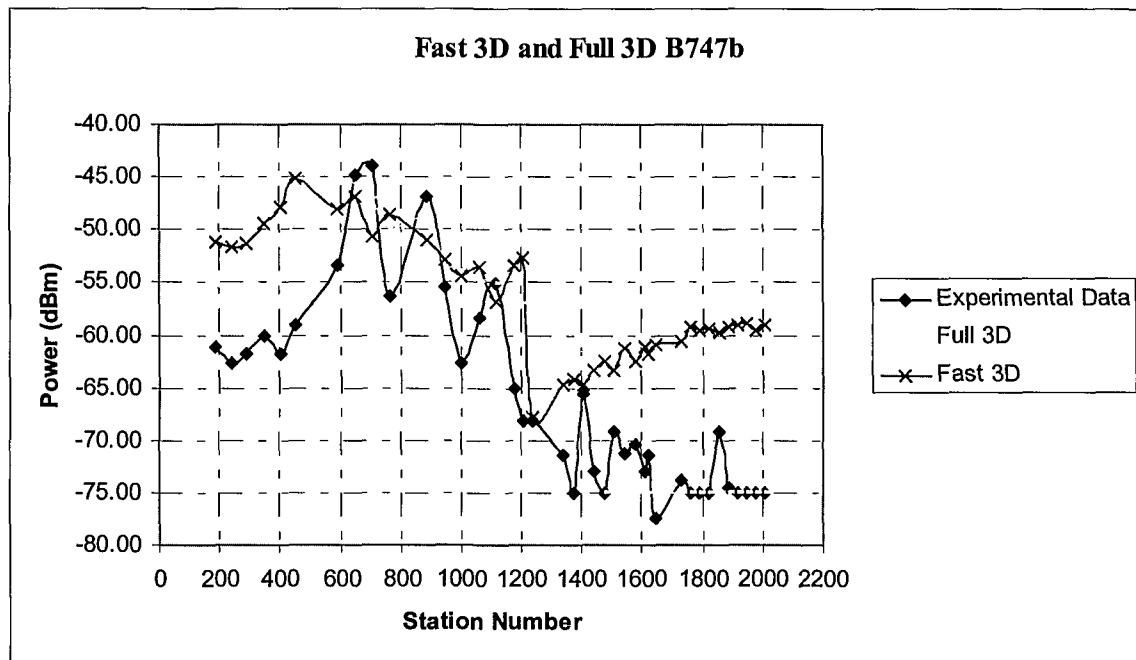
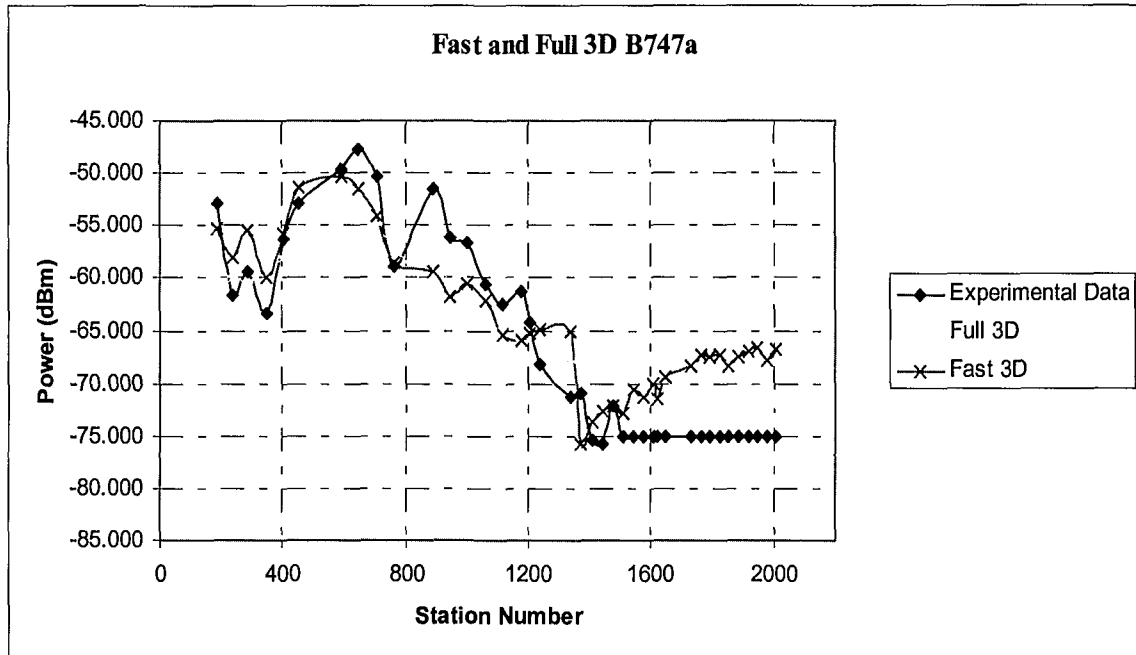
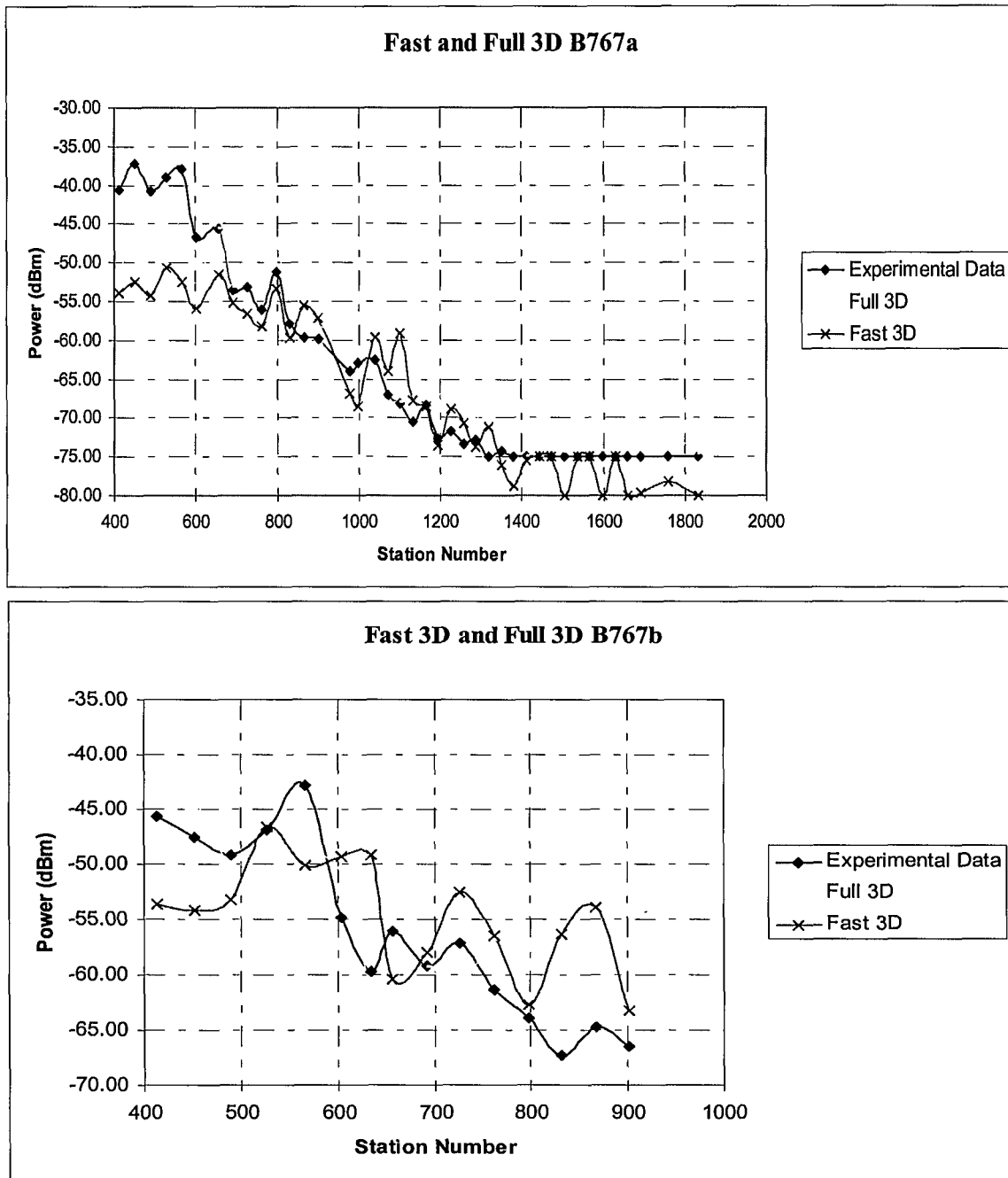


Figure 35: Fast 3D and Full 3D Comparison B747.

Table 14: Table of MAE and RMSE of B747 [Fast 3D and Full3D]

	MAE	RMSE	
Fast 3D	4.379	5.034	B747a
Full 3D	4.200	4.748	
Fast 3D	10.027	11.100	B747b
Full 3D	4.778	6.355	
Experimental Data			



**Figure 36: Fast 3D and Full 3D Comparison B767.**

**Table 15: Table of MAE and RMSE of B767a [Fast 3D and Full 3D]**

	MAE	RMSE	
Fast 3D	4.318	5.992	B747a
Full 3D	4.054	5.272	
Fast 3D	5.564	6.488	B747b
Full 3D	4.186	5.055	
	Experimental Data		

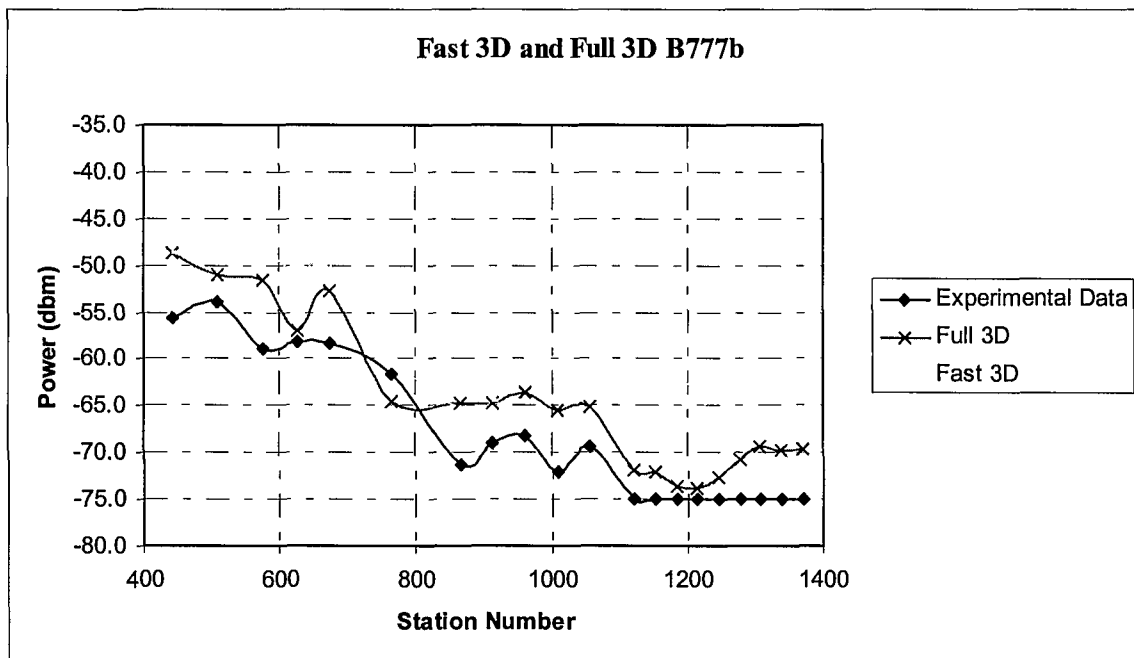
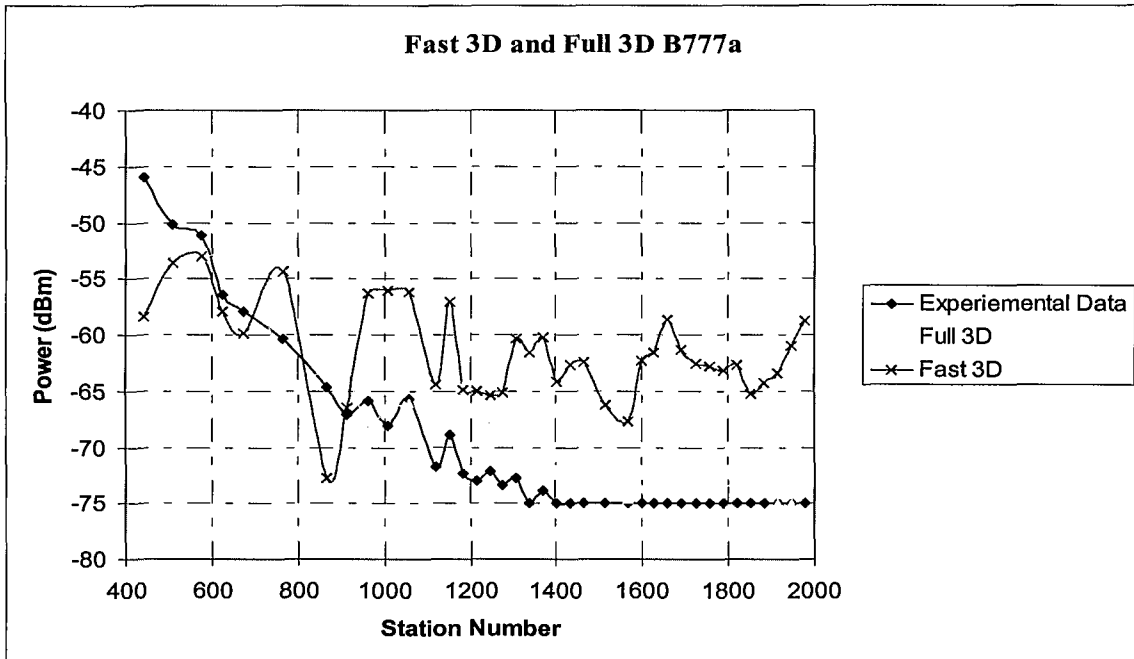


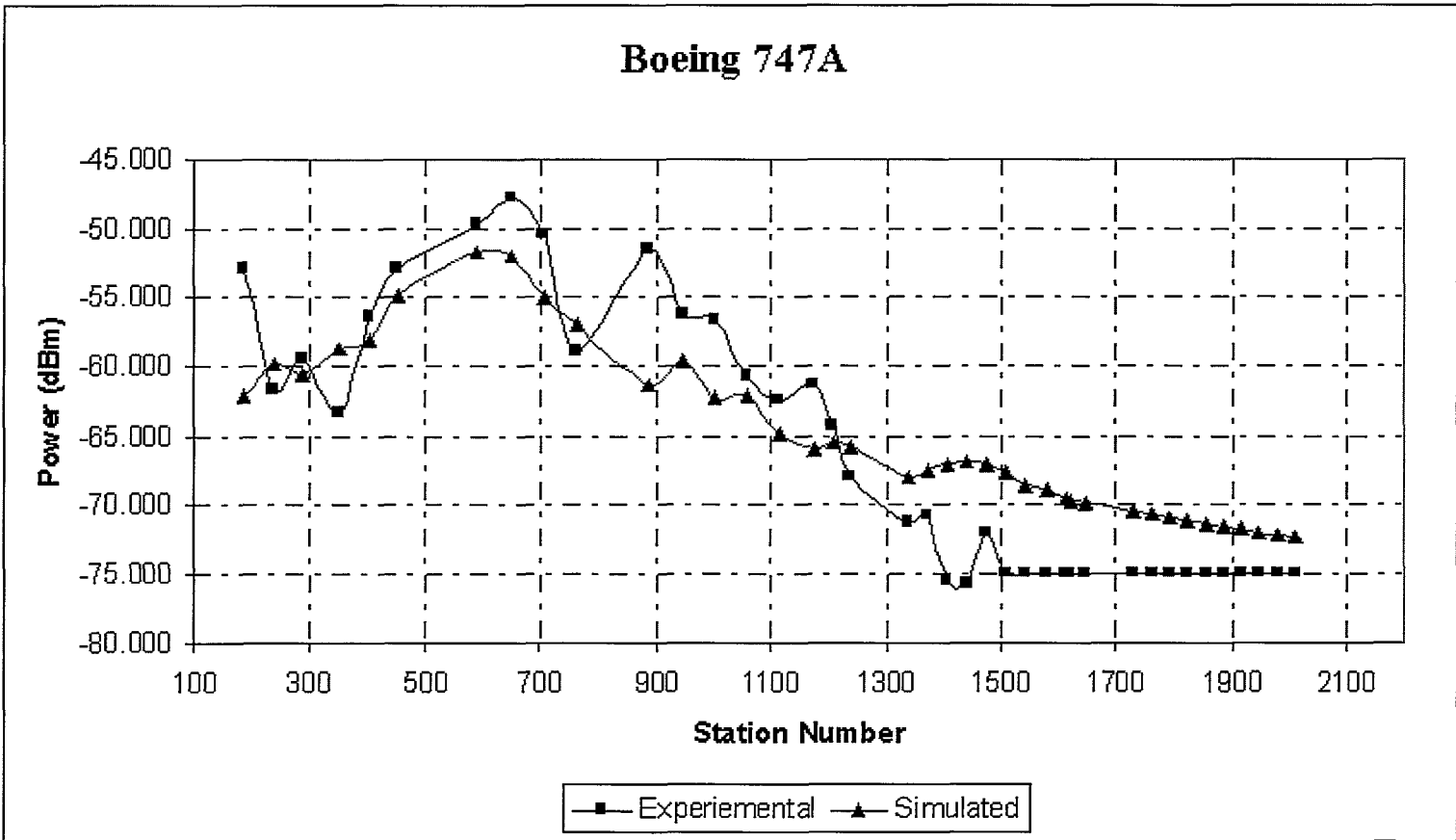
**Figure 37: Fast 3D and Full 3D Comparison B777.**

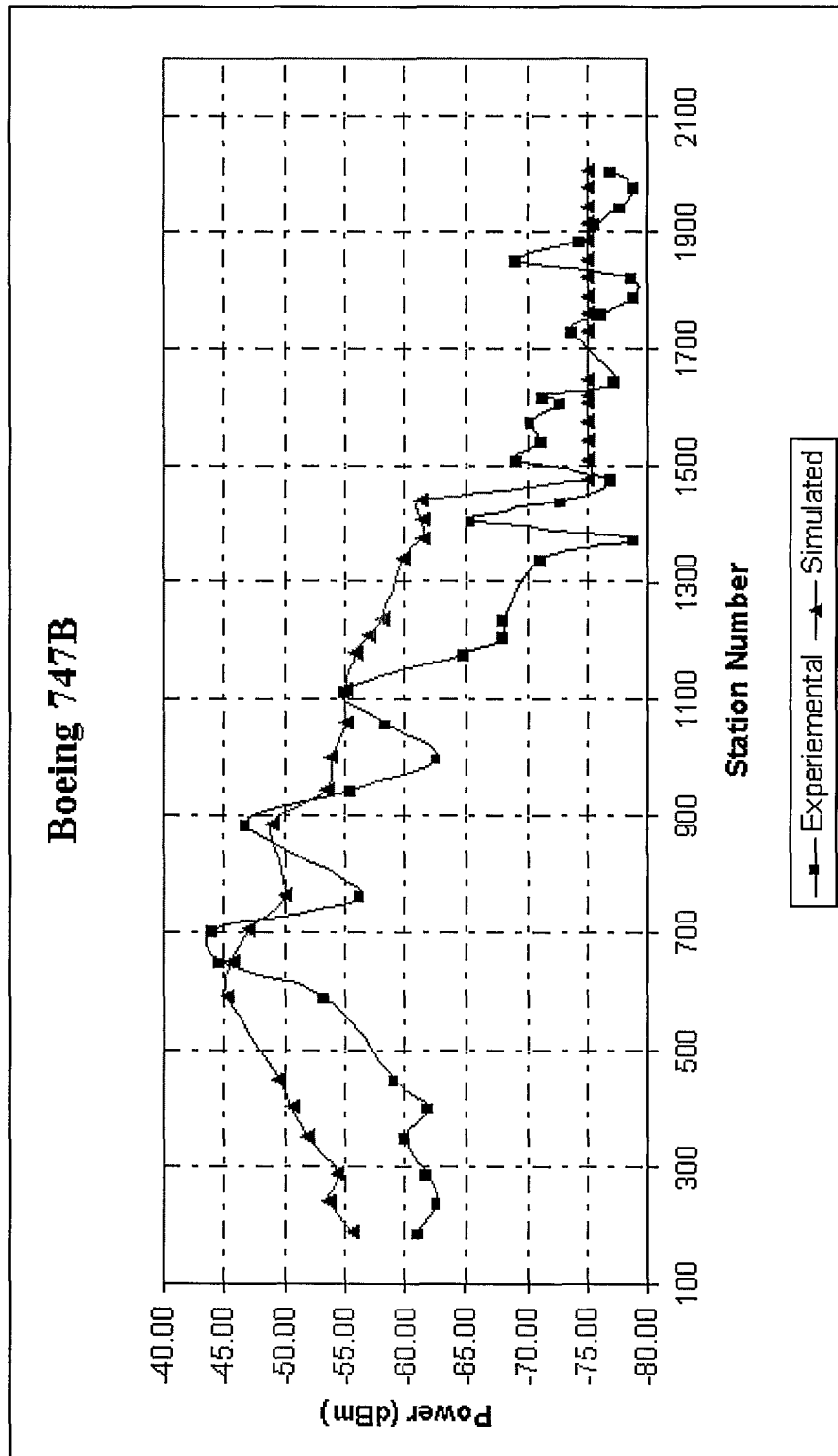
**Table 16: Table of MAE and RMSE of B777 [Fast 3D and Full 3D]**

	MAE	RMSE	
Fast 3D	9.866	10.636	B777a
Full 3D	3.126	3.844	
Fast 3D	9.524	10.160	B777b
Full 3D	4.228	4.632	
Experimental Data			

**Analysis:**

When comparing the Full 3D to the Fast 3D method for the complete fuselage, the error is significantly less for the Full 3D model. Overall the Full 3D method is more accurate. This can be attributed to Full 3D using a 3D trace. It takes into account the shape for complex objects, whereas the Fast 3D method is just an approximation and some objects are neglected. Therefore the results from a Full 3D trace are more dependable than that of a Fast 3D trace. The only factor that may play a role is the running time of each method. On average the Fast 3D method take about 45 to 75 minutes to run. The other method can take anywhere from 60 minutes to 3 hours to run. This time can be reduced in many ways such as reducing the number of faces significantly or reducing the number of reflections that can be accounted for.

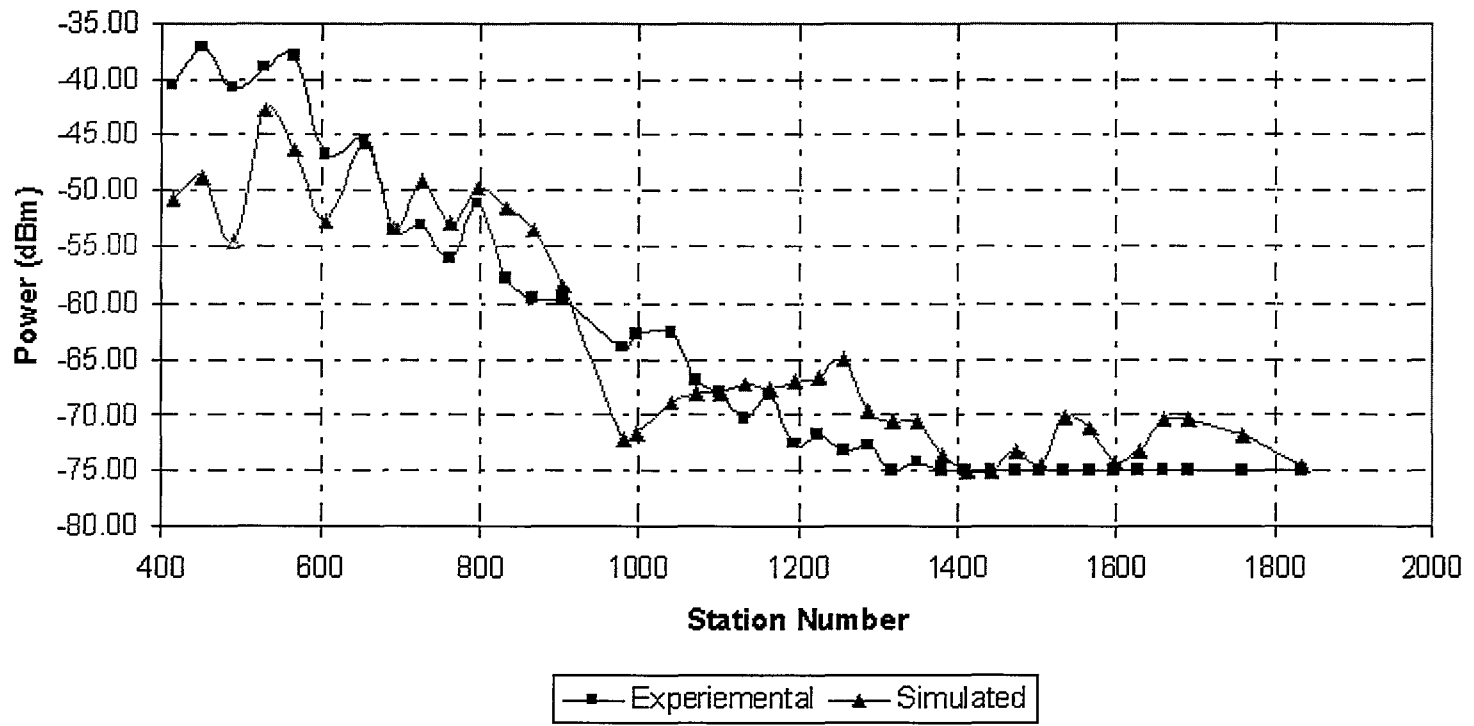


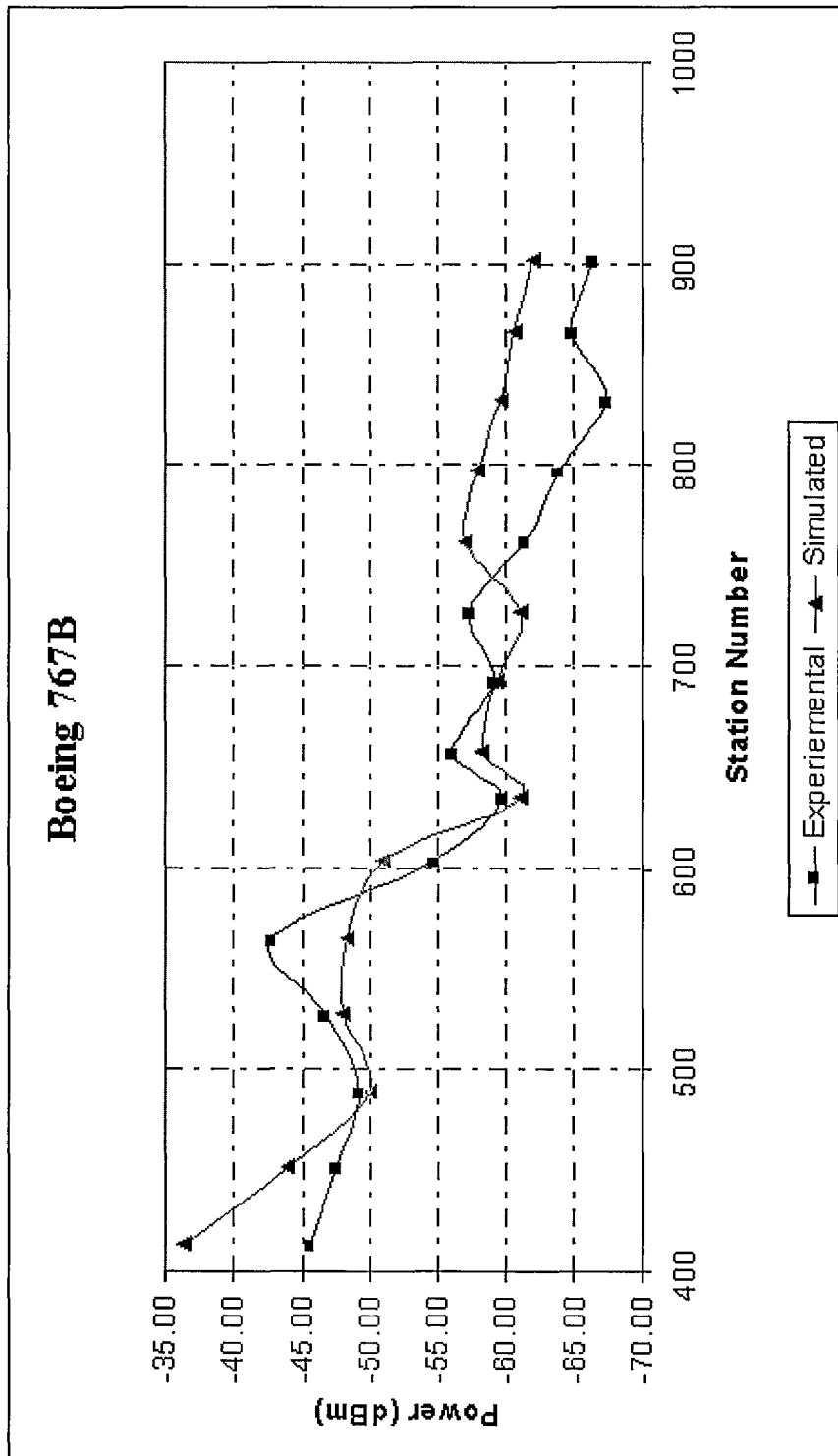


**Figure 38: Comparing 11a and 11b Standard for B747.**  
**Table 17: Comparing 11a and 11b MAE and RMSE for B747**

	MAE	RMSE
802.11a	4.200	4.744
802.11b	4.778	6.355
Experimental Data		

### Boeing 767A

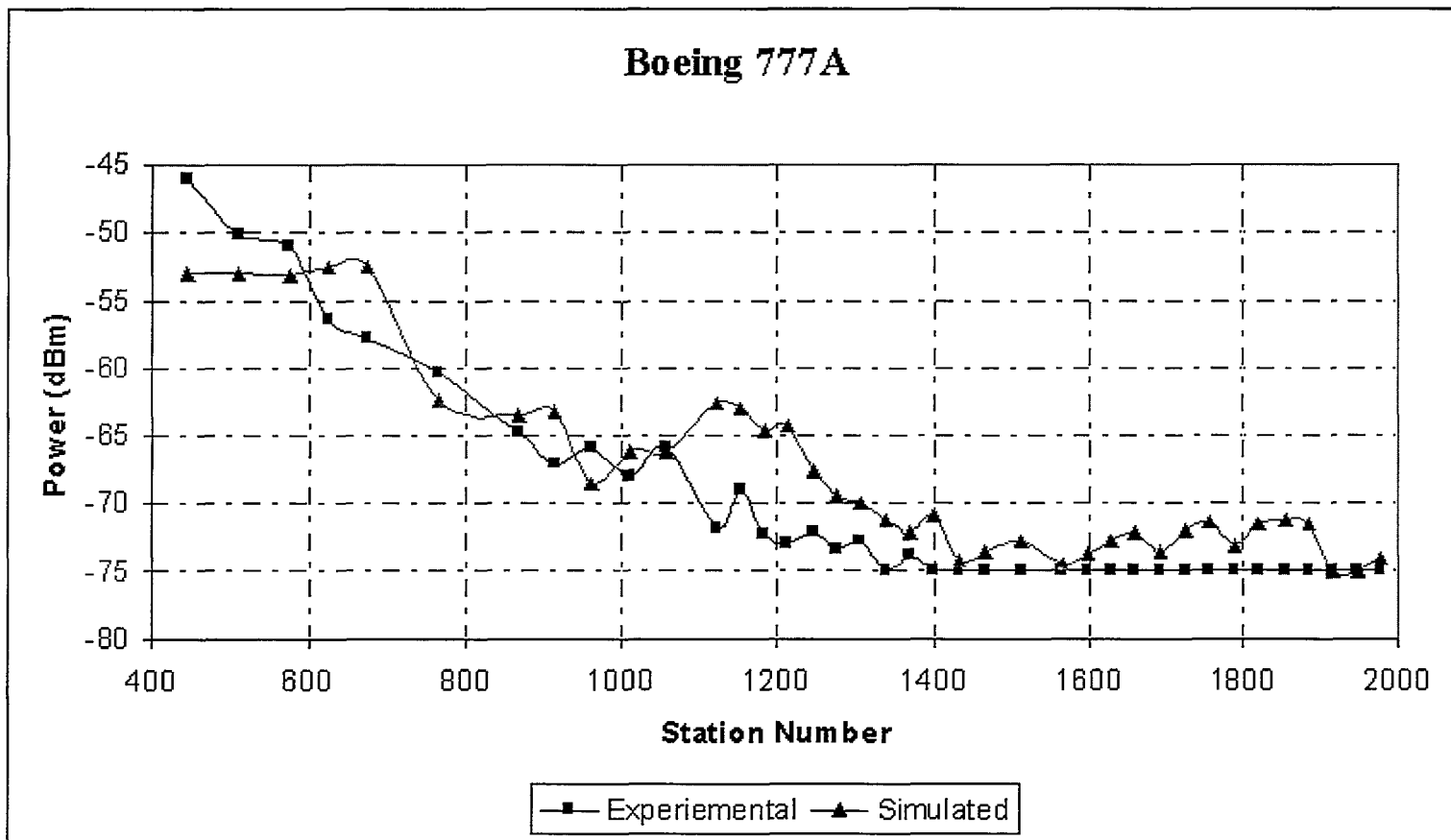




**Figure 39: Comparing 11a and 11b Standard for B767.**

**Table 18: Comparing 11a and 11b MAE and RMSE for B767**

	MAE	RMSE
802.11a	4.504	5.272
802.11b	4.186	5.055
Experimental Data		



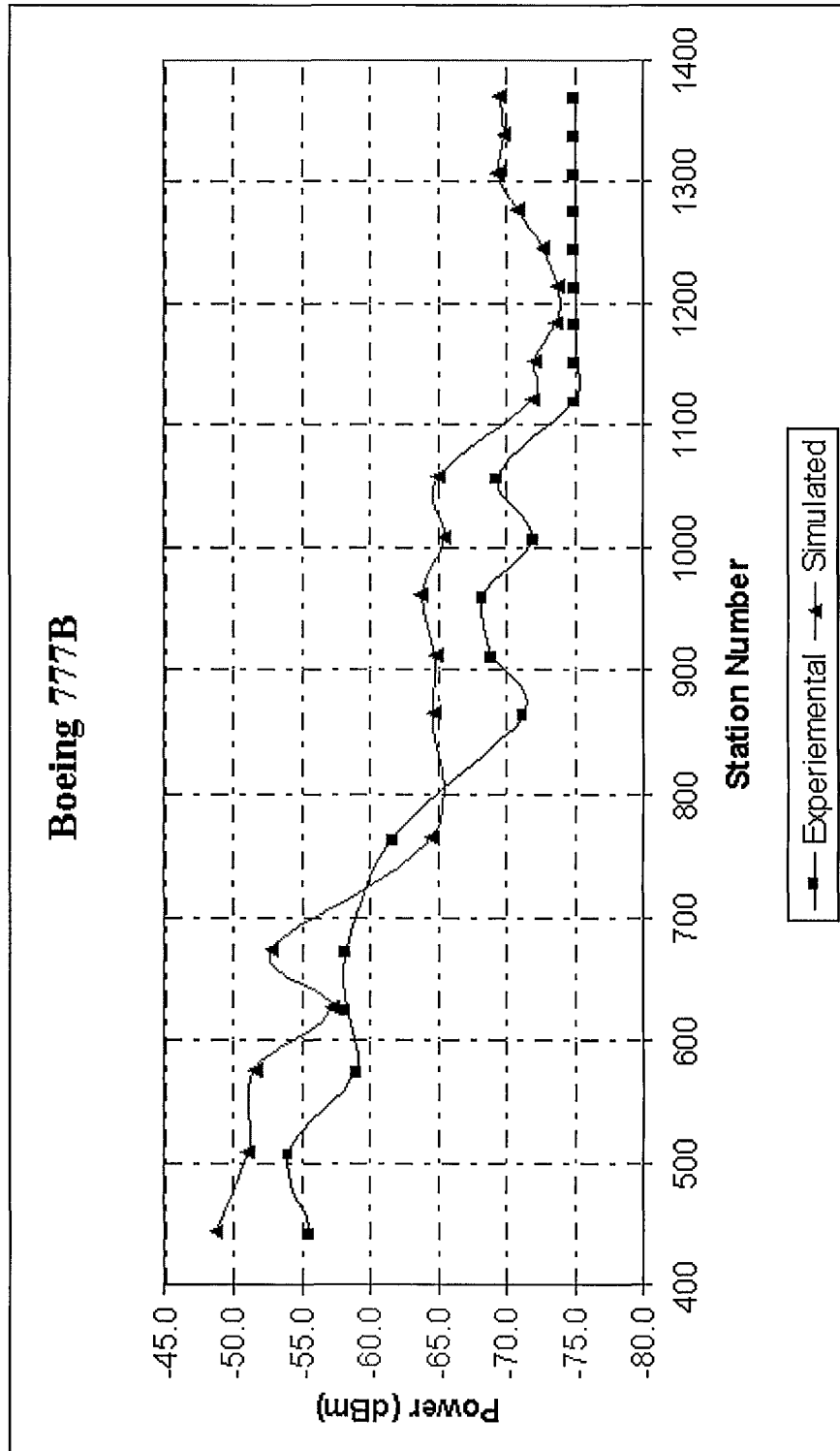


**Figure 40: Comparing 11a and 11b Standard for B777.**

**Table 19: Comparing 11a and 11b MAE and RMSE for B777**

	MAE	RMSE
802.11a	3.126	3.844
802.11b	4.228	4.632
Experimental Data		

## **Analysis:**

The simulated data is that of the completed fuselage with power calculated using the Full 3D method. In all three airplanes the attenuation of the signal is similar to that of the experimental data. This could indicate that the model is accurate. The only difference between the models is the exact power level. This can be attributed back to the material assignments. The MAE of each airplane and standard is less than 5dBm. This is an acceptable error considering that when referring to figures 8 and 9, the spectrum analyzer differed from the client card as much as 10dBm.

## **Possible reasons for differences in experimental data versus simulation**

There are many possible reasons why the experimental data differed from the simulated data. The experimental data environment was not ideal. As mentioned previously, doors were opened, people were moving around, and seats were removed. These would have some effect on the power propagation especially the movement of people. They could potentially stir the electromagnetic waves in the fuselage.

The materials assigned in the fuselage were not the same as those on an actual airplane. The fuselage was assigned as a PEC. Since a PEC reflects all waves and has a transmission coefficient of zero, then the wave propagation would be effected. The receiver and transmitter heights were also estimated from the experimental study. This could also account for some variation in received power [2].

Some other propagation effects can also be taken into account. When the propagation paths were examined in Wireless Insite, there was reflection from the lower compartment noted. Usually this compartment is filled with luggage and other storage

items therefore there should be little or no reflection. Below Figures 32 and 33 show the possible paths the electromagnetic wave takes.



**Figure 41: Propagation Path in B777 [front view].**

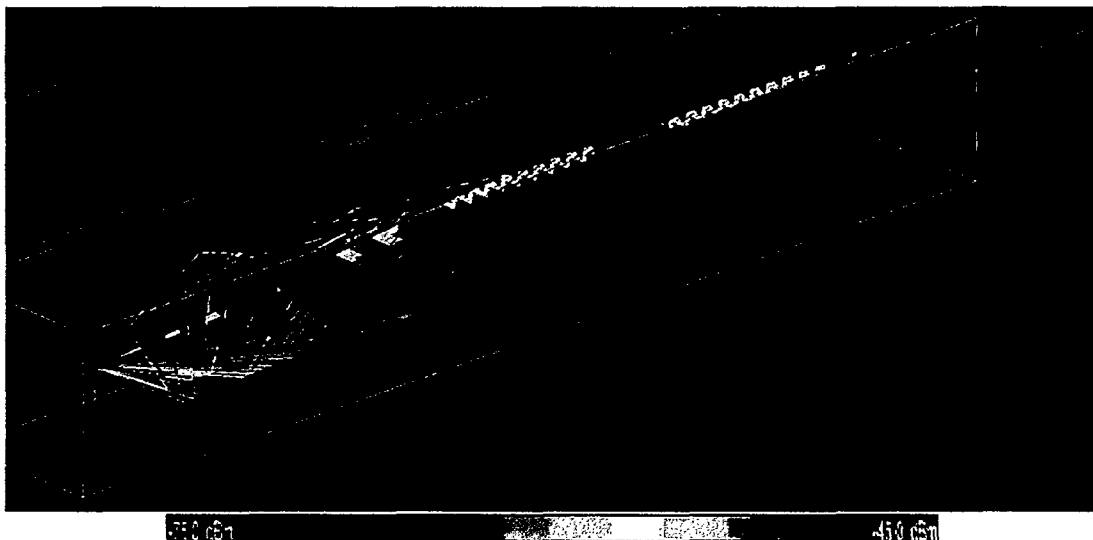


**Figure 42: Propagation Path in B777 [side view].**

## Summary Tables

**Table 1: Summary of B747**

		MAE	RMSE	
Completed Fuselage	B747a	4.379	5.034	Fast 3D
	B747b	10.027	11.100	
Completed Fuselage	B747a	4.200	4.748	Full 3D
	B747b	4.778	6.355	
Empty Fuselage	B747a	6.966	8.344	Fast 3D
	B747b	11.847	13.115	
Empty Fuselage	B747a	4.300	4.744	Full 3D
	B747b	5.082	6.546	
		Experimental Data		

**Table 2: Summary of B767**

		MAE	RMSE	
Completed Fuselage	B767a	4.318	5.992	Fast 3D
	B767b	5.564	6.4888	
Completed Fuselage	B767a	4.054	5.272	Full 3D
	B767b	3.907	4.622	
Empty Fuselage	B767a	4.334	5.903	Fast 3D
	B767b	3.170	3.765	
Empty Fuselage	B767a	4.154	6.124	Full 3D
	B767b	5.796	6.771	
		Experimental Data		

**Table 3: Summary of B777**

		MAE	RMSE	
Completed Fuselage	B777a	9.866	10.636	Fast 3D
	B777b	9.526	10.160	
Completed Fuselage	B777a	3.126	3.844	Full 3D
	B777b	4.228	4.632	
Empty Fuselage	B777a	11.246	12.000	Fast 3D
	B777b	16.406	17.748	
Empty Fuselage	B777a	4.234	4.785	Full 3D
	B777b	5.182	6.150	
		Experimental Data		

## V. CONCLUSIONS

The goal of the present work was to determine if commercial off-the-shelf electromagnetic modeling software could be used to predict electromagnetic propagation inside aircraft cabins. Comparison was made between empty and full fuselage to examine the effects of internal components. The propagation model types [Fast 3D and Full 3D] were also compared for accuracy to experimental study and the IEEE 802.11 standard was examined.

Fuselage model shape was determined to be an important factor. It was found that rectangular models cannot be used as a replacement for cylindrical models. The effect of internal components on power propagation was found to be significant; future models must take into account the internal components. When comparing the two propagation methods, the Full 3D trace was found to be more accurate than the Fast 3D trace.

The results clearly demonstrate that this is possible and quite feasible, and the predictions give good qualitative agreement with experimental data. Furthermore, the level of agreement was surprising, given the level of detail of the aircraft cabin model materials. The models created can serve as prototypes for predicting power in Boeing airplanes.

Future additions to the project could include assigning more detailed material properties to the fuselage. Models could contain humans to determine their effect on the signal propagation. Another interesting thing to examine would be to test all seat locations to determine the power at each location.

## REFERENCES

- [1] Whetten, F.; Soroker, A.; Whetten, D. 802.11 Wireless Network Performances within Aircraft Cabins. Embry-Riddle Aeronautical University: 2003.
- [2] Remcom Incorporated. Wireless Insite User's Manual 2.0.5 December 2004
- [3] Tanenbaum, Andrew. Computer Networks. New York: Prentice Hall PTR, 2003
- [4] Carlson, Bruce, Paul Crilly, and Janet Rutledge. Communication Systems. New York: McGraw Hill, 2001
- [5] Ramsey, James, "Wireless Undeterred."  
[http://avionicsmagazine.com/cgi/av/show\\_mag.cgi?pub=av&mon=0204&file=0204wireless.htm](http://avionicsmagazine.com/cgi/av/show_mag.cgi?pub=av&mon=0204&file=0204wireless.htm) 4 February 2004. 12 January 2005
- [6] W.K. Tam and V.N. Tran. Multi-ray propagation model for indoor wireless communications. *Electronics and Communication Engineering Journal*, 32:135–137, Jan 1996.
- [7] Damasso, E., Paraboni, A., Protto, F., "Indoor propagation measurements: application to mobile channel modeling", 8th Int. Conf. on Antennas and Propagation, Edinburgh, UK, March 1993
- [8] Yee, K. S.: Numerical solution of initial boundary value problems involving Maxwell's equations in isotropic media. *IEEE Transactions: Antennas Propagation*, Vol. 14, pp 302-307, May 1966.
- [9] Rappaport, T.S., Annamalai, A., Buehrer, R.M., and Tranter, W.H.: 'Wireless communications: past events and future perspective', *IEEE Communication Magazine*., 50th Anniversary Commemorative Issue, May 2002
- [10] Jahn, A.; et al. :'Evolution of aeronautical communications for personal and multimedia services' *Communications Magazine*, IEEE Volume 41, Issue 7, July 2003 Page(s):36 – 43
- [11] D. Dobkin. "Indoor propagation issues for wireless LANs." *RF Design*; [www.rfdesign.com](http://www.rfdesign.com), Sep 2002. 12 January 2005.
- [12] Homepage. Boeing. April 2, 2005. Boeing. { <http://www.boeing.com/flash.html> }
- [13] Homepage. Federal Communication Commission. April 2, 2005. FCC. { <http://www.fcc.gov/> }

## VITA

### MENNATOALLAH YOUSSEF

#### EDUCATION

Master of Science (Electrical Engineering), Old Dominion University, Norfolk, VA, August 2005

Bachelor of Science (Electrical Engineering), Old Dominion University, Norfolk, VA, May 2004

#### EXPERIENCE

Department of Electrical and Computer Engineering, Old Dominion University, Norfolk, VA

Graduate Teacher Assistance, March 2005 – May 2005

NASA Langley, Hampton, VA

Graduate Research Assistant, May 2004 – May 2005

Department of Electrical and Computer Engineering, Old Dominion University, Norfolk, VA

Graduate Teacher Assistant, January 2004 – May 2004

Department of Electrical and Computer Engineering, Old Dominion University, Norfolk, VA

Graduate Teacher, April 2005 – May 2005

#### SCIENTIFIC AND HONOR SOCIETIES MEMBERSHIP

Member of Tau Beta Pi, Engineering Honor Society

Member of Institute of Electrical and Electronics Engineers

#### SCHOLARLY ACTIVITIES

Mennatoallah Youssef, Linda Vahala, John Beggs, “Wireless Network Simulation in Aircraft Cabins,” IEEE Antennas and Propagation Society International Symposium, July 2004. Monterey, California

Mennatoallah Youssef, Linda Vahala, John Beggs, “Electromagnetic Propagation of Wireless Networks in Aircraft Cabins,” 2005 IEEE/ACES International Conference on Wireless Communication and Applied Computational Electromagnetics, April 2005. Honolulu, Hawaii